



Geologic mapping of Vesta

R.A. Yingst^{a,*}, S.C. Mest^a, D.C. Berman^a, W.B. Garry^a, D.A. Williams^b, D. Buczkowski^c,
R. Jaumann^d, C.M. Pieters^e, M.C. De Sanctis^f, A. Frigeri^f, L. Le Corre^g, F. Preusker^d,
C.A. Raymond^h, V. Reddy^g, C.T. Russellⁱ, T. Roatsch^d, P.M. Schenk^j

^a Planetary Science Institute, 1700 E. Ft. Lowell, Suite 106, Tucson, AZ 85719, United States

^b Arizona State University, AZ, United States

^c JHU-APL, MD, United States

^d DLR, Institute of Planetary Research, Berlin, Germany

^e Brown University, RI, United States

^f National Institute of Astrophysics, Italy

^g Max Planck Institute for Solar System Research, Germany

^h NASA JPL, California Institute of Technology, CA, United States

ⁱ UCLA, CA, United States

^j LPI, TX, United States

ARTICLE INFO

Article history:

Received 14 February 2013

Received in revised form

25 November 2013

Accepted 21 December 2013

Available online 3 January 2014

Keywords:

Dawn

Vesta

Geologic mapping

ABSTRACT

We report on a preliminary global geologic map of Vesta, based on data from the Dawn spacecraft's High-Altitude Mapping Orbit (HAMO) and informed by Low-Altitude Mapping Orbit (LAMO) data. This map is part of an iterative mapping effort; the geologic map has been refined with each improvement in resolution. Vesta has a heavily-cratered surface, with large craters evident in numerous locations. The south pole is dominated by an impact structure identified before Dawn's arrival. Two large impact structures have been resolved: the younger, larger Rheasilvia structure, and the older, more degraded Veneneia structure. The surface is also characterized by a system of deep, globe-girdling equatorial troughs and ridges, as well as an older system of troughs and ridges to the north. Troughs and ridges are also evident cutting across, and spiraling arcuately from, the Rheasilvia central mound. However, no volcanic features have been unequivocally identified. Vesta can be divided very broadly into three terrains: heavily-cratered terrain; ridge-and-trough terrain (equatorial and northern); and terrain associated with the Rheasilvia crater. Localized features include bright and dark material and ejecta (some defined specifically by color); lobate deposits; and mass-wasting materials. No obvious volcanic features are evident. Stratigraphy of Vesta's geologic units suggests a history in which formation of a primary crust was followed by the formation of impact craters, including Veneneia and the associated Saturnalia Fossae unit. Formation of Rheasilvia followed, along with associated structural deformation that shaped the Divalia Fossae ridge-and-trough unit at the equator. Subsequent impacts and mass wasting events subdued impact craters, rims and portions of ridge-and-trough sets, and formed slumps and landslides, especially within crater floors and along crater rims and scarps. Subsequent to the formation of Rheasilvia, discontinuous low-albedo deposits formed or were emplaced; these lie stratigraphically above the equatorial ridges that likely were formed by Rheasilvia. The last features to be formed were craters with bright rays and other surface mantling deposits. Executed progressively throughout data acquisition, the iterative mapping process provided the team with geologic proto-units in a timely manner. However, interpretation of the resulting map was hampered by the necessity to provide the team with a standard nomenclature and symbology early in the process. With regard to mapping and interpreting units, the mapping process was hindered by the lack of calibrated mineralogic information. Topography and shadow played an important role in discriminating features and terrains, especially in the early stages of data acquisition.

© 2014 Elsevier Ltd. All rights reserved.

1. Introduction

Geologic mapping is a comprehensive investigative process that organizes disparate datasets into geologic units with the goal of revealing the underlying geologic processes and placing those

* Corresponding author. Tel.: +1 920 360 3627; fax: +1 920 465 2376.
E-mail address: yingst@psi.edu (R.A. Yingst).

processes into a global, contextual framework. The arrival of the Dawn spacecraft at the asteroid Vesta provides a first opportunity for this approach to be utilized for Vesta at the sub-km scale, at which features such as impact craters, local landslides and tectonic structures can be resolved. The inner main belt asteroid Vesta is a particularly compelling target for this traditional investigative process because of long-standing evidence for its basaltic surface and longitudinal mineralogic heterogeneity gathered first through Earth-based polarimetric and spectroscopic measurements (Degewij et al., 1979; Gaffey, 1997, 1983; McCord et al., 1970; Reddy et al., 2010). Such a surface indicated a differentiated crust and, potentially, volcanic activity in Vesta's past.

Prior to the arrival of the Dawn spacecraft, the highest-resolution images of the surface of Vesta (38 km/pixel) were provided by the Hubble Space Telescope (HST; Li et al., 2010). During favorable approach conditions in 1994 and 1996, the HST provided reflectance data at 0.439, 0.673, 0.953 and 1.042 μm , and from these data, albedo, elevation and mineralogical data were derived, from which maps of mineralogic composition and lithology were produced (Binzel et al., 1997; Gaffey, 1997; Li et al., 2008, 2006). These data revealed a surface dominated by regionally distinct units interpreted to be impact-excavated pyroxene-rich plutonic material, results that agreed generally with mineralogic maps created from Earth-based spectroscopy (Degewij et al., 1979; Gaffey, 1997, 1983; Reddy et al., 2010). Though necessarily generated from images with a resolution no better than 38.5–52 km/pixel (Binzel et al., 1997; Li et al., 2010, 2008; Zellner et al., 1997), these maps represented first steps in understanding Vesta's geologic history.

NASA's Dawn spacecraft entered Vestan orbit on July 16, 2011, and spent one year in orbit to characterize its geomorphology, elemental and mineralogical composition, topography, shape, and internal structure before departing to asteroid Ceres on September 5, 2012. Three orbital phases of the mission returned images at successively higher resolutions; the highest of these was 20–25 m/pixel. Preliminary geologic results from the initial orbital phase ("Survey orbit") are reported by Russell et al. (2012) and Jaumann et al. (2012).

During the pre-encounter phase of the mission, the Dawn science team followed the recommendations of Batson (1990) for planetary geologic mapping and divided the asteroid into 15 quadrangles for geologic mapping. Preliminary global geologic maps were also produced in an iterative fashion as new data became available (Yingst et al., 2012, 2011). These iterations of the global geologic map were utilized by the science team during the active phases of the mission to inform evolving hypotheses, correlate crater size-frequency statistics, mineralogic data and other products with preliminary geologic units, and place new data within a baseline geologic context. This work represents the compilation and analysis of these iterative efforts.

2. Approach

A geologic map is a visual representation of the distribution and sequence of rock types and other geologic information. It allows observations to be organized and represented in an intuitive format, unifies observations of heterogeneous surfaces made at different localities into a comprehensive whole, and provides a framework for science questions to be answered. A geologic map defines boundaries for the extent and overlap of important characteristics such as mineralogy, topography, morphology and elemental abundance. This information can then be used to analyze relationships between these characteristics; this, in turn, can inform models of thermal and structural evolution. In the case of Vesta, a geologic map also would allow the HED

(howardite, eucrite and diogenite) meteorites (a family of meteorites believed to have originated from Vesta (Binzel and Xu, 1993; Consolmagno and Drake, 1977; McCord et al., 1970) and discussed in more detail in Section 3) to be placed in geologic context, should the sources be located.

The goals in creating any geologic map determine the level of detail at which the map is created, and thus the required spatial resolution of data selected for the base map. Where the goal is to summarize the current state of knowledge for a region for archiving, the presented map will differ from one where the purpose is to provide a preliminary overview of geologic context in a setting where data collection is in process, or where the amount or type of data available varies across the mapped region. These latter maps are often iterative – that is, multiple versions are created because each iteration is refined as data become available. An example of such a situation is the geologic mapping that may occur during field work, where a sketch map of local units or layers is created first to inform the choice of future sampling locations, and is updated as those samples are collected and analyzed. The more comprehensive geologic map is generated later, when all the available data has been acquired, refined and analyzed in detail.

An orbital mission to another planetary body is analogous to this scenario of field work followed by data analysis, where time in the field mirrors the period of spacecraft data acquisition. A detailed geologic map is often generated after the mission ends, once all the data are acquired and have been fully calibrated and refined. However, as in field work, analysis of data begins as soon as it is acquired. Iterative mapping is a process that provides the geologic context for, and reveals the interrelationships of, geologic characteristics revealed by each emerging dataset. Further, it can do so within a timeframe that allows the map to inform data analysis of other team members on the mission timeline.

The global geologic maps presented here demonstrate the progression of lessons learned from generating each iteration (Yingst et al., 2012, 2011). Where possible, we have referred back to units and surface features identified by mapping efforts that predate the Dawn mission (Binzel et al., 1997; Gaffey, 1997); we note that because the spatial resolution available for these mapping efforts was ~ 500 times coarser than that available here, there are previously named and mapped regions that are not included because they do not exist as geologically defined features. This includes Olbers Regio, identified in HST images as a dark ovoid region approximately 200 km across. For the final iteration of the map we include type examples of units and landforms, and descriptions and interpretations of primary units; we also attempt to deconvolve and interpret the basic stratigraphy in a relative sense utilizing stratigraphic relationships. We intend for the map to provide a contextual framework for more advanced compositional and/or geomorphological mapping at large scales (smaller regions). However, because the process of data analysis is still in its early stages as of this writing, we expect the concepts for the units and structures presented to evolve as analysis and understanding mature. Our goals for this work are thus twofold: firstly, to provide the community with a preliminary assessment of the geology of Vesta, using traditional geologic mapping methods as a primary tool to perform this assessment; and secondly, to report on and analyze the mapping process as it was conducted during an active mission, where iterative products were fed directly to the team to inform subsequent data acquisition and analysis.

3. Geologic setting

Vesta is an ellipsoidal asteroid with dimensions estimated at $286.3 \times 278.6 \times 223.2 \pm 0.1$ km (Russell et al., 2012). Efforts by

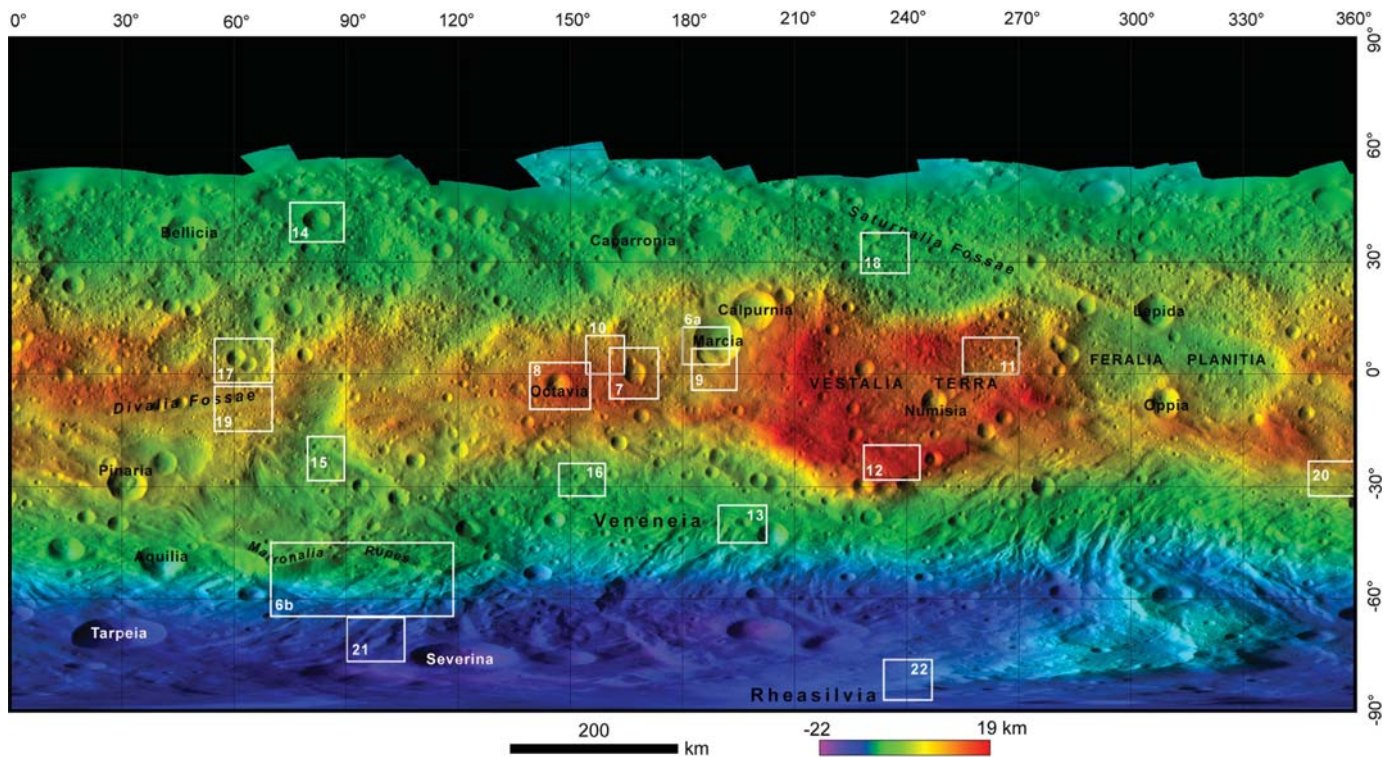


Fig. 1. Color shaded relief map of the surface of Vesta. Topography is derived from Dawn Framing Camera data. The coordinate system shows is the “Claudia” system used by the Dawn science team. The map shows the locations of physiographic provinces, major structural centers and impact structures greater than 30 km in diameter. White boxes indicate the locations of type Figs. 6–22 throughout the paper. (For interpretation of the references to color in this figure legend, the reader is referred to the web version of this article.) Image credit: NASA/JPL/DLR.

Binzel et al. (1997), Gaffey (1997) and Li et al. (2010, 2008) utilized Earth-based and HST spectral data to identify and interpret low-resolution albedo patterns on the surface. Spectral signatures were also identified based on ground-based spectroscopy and HST Wide-Field Planetary Camera (WFPC2) images that resolved Vesta at up to $\sim 9^\circ/\text{pixel}$. Characteristics used to discriminate between potential units included derived albedo, spectral shape, and variations in the depth, position and width of the $1\ \mu\text{m}$ absorption band (Fe^{2+} , a common component of basaltic minerals, has a $1\ \mu\text{m}$ absorption band). The lithologic maps derived from analysis of these data showed a surface composed of several discrete, spectrally-similar regions. The hemisphere that Binzel et al. (1997) noted as their “western hemisphere” was interpreted as relatively uniform, similar to iron-rich pyroxenes, and comparable to surface basalts such as eucrite meteorites. By contrast, their “eastern hemisphere” was more diverse, with magnesium-rich pyroxenes and several regions of olivine-rich, diogenite, and low-Ca eucrite regions located near the prime meridian (Binzel et al., 1997; Gaffey, 1997). The average surface of Vesta was noted as analogous to a mix of howardite or polymict eucrite; these are regolith-derived members of the HED meteorites (Gaffey, 1997). These results indicated that Vesta has an old, differentiated surface, with spectrally-distinct regions that can be geochemically tied to the HED meteorites. Crystallization ages measured by radiometric dating for HEDs in Earth-based laboratories document that rocks comprising Vesta were formed within the first 100 million years of solar system history (4.43–4.55 Gyr; Lugmair and Shukolyukov, 1998; Nyquist et al., 1997; Tera et al., 1997; see review by McSween et al., 2011). The mapping results reveal surface features formed by processes that must postdate the very old age of the HEDs.

Data available prior to the Dawn mission indicated that impact cratering was the dominant process on the surface of Vesta (e.g., Gaffey, 1997), and the Dawn data confirm that Vesta has a heavily-cratered surface (e.g., Marchi et al., 2012a). The south pole is

dominated by a large impact structure identified before Dawn’s arrival (Thomas et al., 1997a,b); the name Rheasilvia has been approved by the International Astronomical Union (IAU) for this structure (the IAU is the organization that certifies the nomenclature of planetary features; only IAU-approved names are used throughout this manuscript). The surface also has three large systems of troughs and ridges: one around the equator, one confined to the northern hemisphere, and one cutting across, and spiraling arcuately from, the Rheasilvia central mound (Jaumann et al., 2012). A color relief map of the surface is shown in Fig. 1.

Global geologic mapping and image analysis of Vesta using data of increasing resolution acquired at successive phases of the Dawn mission has enabled the identification of several impact basins hundreds of kilometers in diameter (e.g., Rheasilvia, Veneneia), an ancient heavily cratered northern hemisphere, and regional sets of graben and ridge-and-groove structures (e.g., Divalia Fossae and Saturnalia Fossae). We have also mapped and characterized a number of geologic units associated with impact basins and craters, regional cratered plains and highlands units, and surficial deposits suggesting localized mass wasting of loose material.

4. Data and mapping procedure

Each of Dawn’s several orbital phases at Vesta provided increasingly higher spatial resolution data that were integrated into the mapping effort, as summarized in Table 1. Using data from each of these phases as “waypoints,” we completed three main iterations of the global map. The first was created during the approach phase, when data were taken to determine the Vestan pole (Rotational Characterization, or RC) and to support navigation (Optical Navigation, or OpNav). The RC/OpNav map was based on clear filter data from the Framing Camera (FC), which covered the surface at 3–9 km/pixel resolution. The second iteration was

completed subsequent to Survey orbit and was based on FC clear filter data at ~ 200 m resolution and a Digital Terrain Model (DTM) derived from Survey orbit image data (Jaumann et al., 2012; Preusker et al., 2012). The third was based on data from the High-Altitude Mapping Orbit (HAMO) with a spatial resolution of ~ 61 m/pixel. For a summary of the navigational aspects of the Dawn at Vesta mission, including orbit tracks, see Russell et al. (2005) and Polansky et al. (2011).

The preparation of all iterations of the geologic map followed the methods developed and described by Shoemaker and Hackman (1962), Wilhelms (1990, 1972), Tanaka et al. (1994, 2010) and Greeley and Batson (1990). Units were defined on the basis of characteristics such as morphologic features, surface textures, color and albedo; where color is defined as the color ratio scheme used in Clementine multispectral images (Clementine data are often displayed as ratios of $415/750 \mu\text{m}$ in red, $750/950 \mu\text{m}$ in green, and $750/$

$415 \mu\text{m}$ in blue; here we use $440/750 \mu\text{m}$, $750/920 \mu\text{m}$ and $750/440 \mu\text{m}$).

For the first iteration (RC/OpNav), the portion of the surface imaged was mapped in its entirety by four separate workers who then compared and consolidated results. This method was adopted for two reasons: Firstly, it was important in this early stage to allow all mappers to become familiar with the surface features as rapidly as possible, as the first map had to be produced within a few months. Secondly, we wanted to calibrate the different approaches that each mapper utilized, so that in later iterations this would be a relatively known factor.

For the second iteration, each worker mapped one of four broad regions: $30\text{--}90^\circ\text{S}$, or $0\text{--}120^\circ$, $120\text{--}240^\circ$ or $240\text{--}360^\circ$ longitude, with each of the latter three blocks ranging from 30°S latitude to the limit of coverage in the north. Some overlap occurred where features or units straddled these longitudinal blocks; this overlap allowed the mappers to compare results and address any potential areas of disagreement. For the third iteration, each worker mapped a different one of these longitudinally-defined blocks, to lessen bias and to allow each worker to become familiar with the geology of the entire body at significantly higher resolution than revealed by RC/OpNav.

Table 1

Datasets utilized in the mapping effort. The resolutions acquired for each orbit are noted.

	RC/OpNav	Survey	HAMO
Framing Camera, mosaic	400 m/pixel	250 m/pixel	60 m/pixel
DTM	750 m/pixel	445 m/pixel	92 m/pixel
Geologic mapping scale	1:20–25 M	1:1 M	1:500 K

4.1. Iterative mapping

4.1.1. RC/OpNav iteration

The initial iterations of the map, based on FC images from the OpNav and Survey phases of the mission, were generated in Adobe

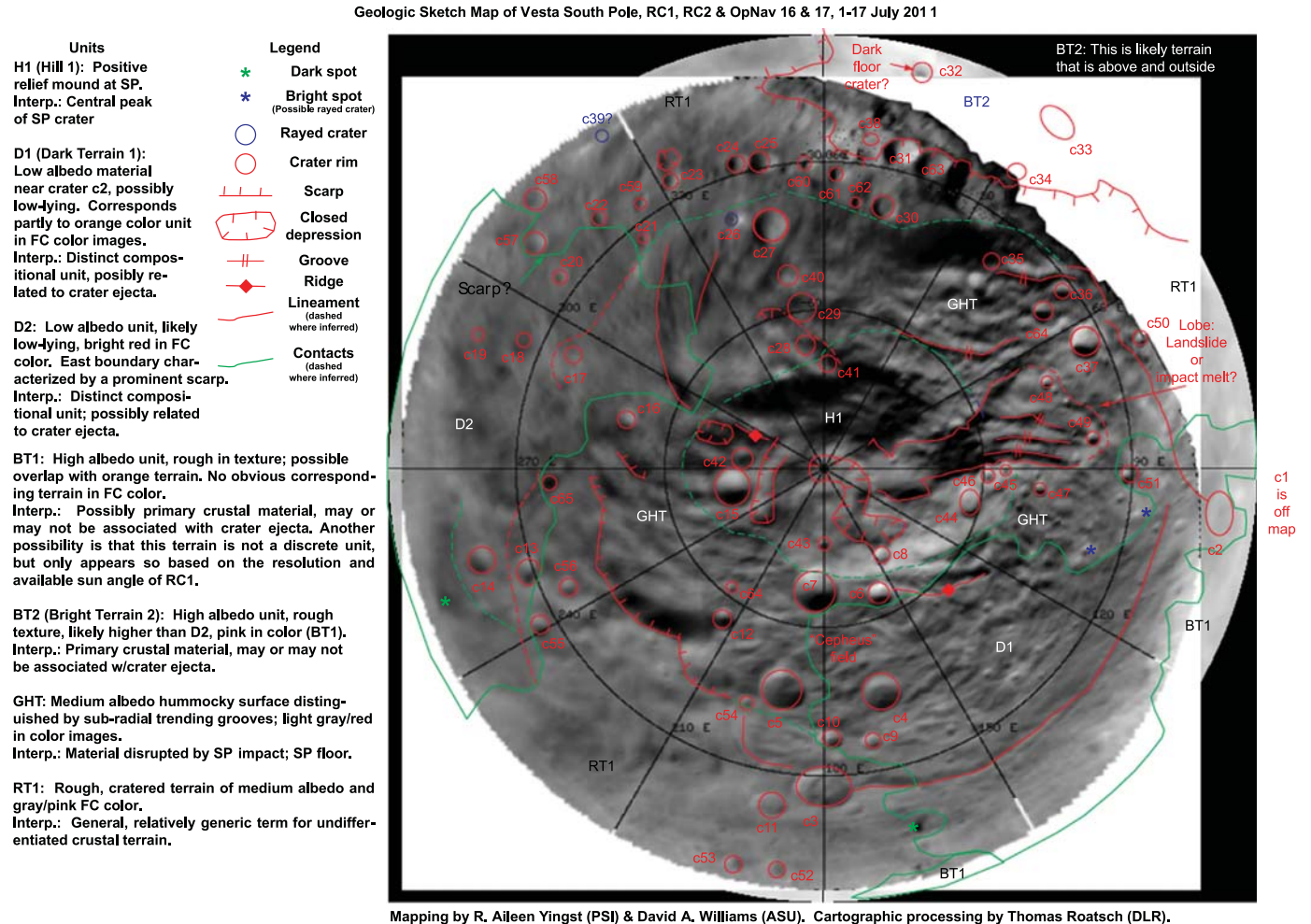


Fig. 2. Map of Vesta's southern hemisphere based on Framing Camera Rotational Characterization (RC) data. The latitude/longitude coordinate system shown is an arbitrary set of longitudes overlaid (the FC team had not settled on a standard latitude/longitude system at this time).

Illustrator by the mapping team. The map produced from RC and OpNav data is shown in Fig. 2. This map covers latitudes from 0 to 90°; however, RC/OpNav data covered some areas further north than the equator. Units are informed by these more northern images. Hypotheses to be tested in this iteration were that the surface of Vesta would show evidence of two processes: (1) cratering, especially in the form of a large crater at or near the south pole; and (2) volcanism, in the form of some surface features, possibly vents and flows (as predicted by Wilson and Keil, 1996), or pyroclastic material.

In this iteration of the map, we divided the surface into brighter- and darker-toned units, as well as circular features that were inferred at the time (and later confirmed) to be impact craters. Large variations in topography were also visible, including several prominent scarps. Other features identified included the south polar impact crater (Rheasilvia) and two ridges identified in later iterations as the scarp discontinuously bounding the crater (ridge1 and ridge2 in Fig. 2); lower-albedo regions associated with Rheasilvia ejecta (d1); a high plateau (BT2, Vestalia Terra); and grooves within the Rheasilvia impact structure (noted as GHT in Fig. 2, with individual troughs outlined where they could be identified). Prominent features on Vesta that could not be discerned at this resolution included Veneneia and all other, smaller craters. The large topographic variation from the top of Vestalia Terra to the bottom of the craters Marcia, Calpurnia and Minucia was noted but we mapped it incorrectly in this iteration as a crater rim (the

eastern rims of the three craters combined) and a potential complex crater peak (the high-standing rim of Marcia and Calpurnia, which were among the highest albedo features seen at this resolution; see Fig. 3). This combination of features likely represents what was originally identified as the dark albedo feature “Olbers Regio” on previous maps, as noted by Reddy et al. (2012a,b, 2013). Notably, though the ridge-and-trough system around the equator is very prominent, it was not identified or mapped at this resolution (the northern latitudes were not imaged at this altitude). The walls of the deepest troughs, which could be seen in some of the earliest FC images, were mapped as curved crater rims. In terms of color ratio data (defined as FC monochrome data and color ratio data, where red–blue tones capture the visible continuum and green tones capture the relative strength of the ferrous absorption band at 1.0 μm), the most prominent feature noted was a deposit that appears orange-toned. This feature was first identified in the images shown in Fig. 3, and inferred to be associated with a nearby circular feature (confirmed as an impact crater in Survey data, and named Octavia). Its location is broadly similar to that of a potential olivine signature noted by Binzel et al. (1997). In this iteration we mapped the deposit as a surface mantling feature, pending more detailed morphologic data. We note, however, that another prominent “orange” toned deposit that was revealed in the Survey data around the crater Oppia does not correlate with any spectral signature noted by Binzel et al. (1997). These types of deposits are discussed in more depth in Section 5.5.1.

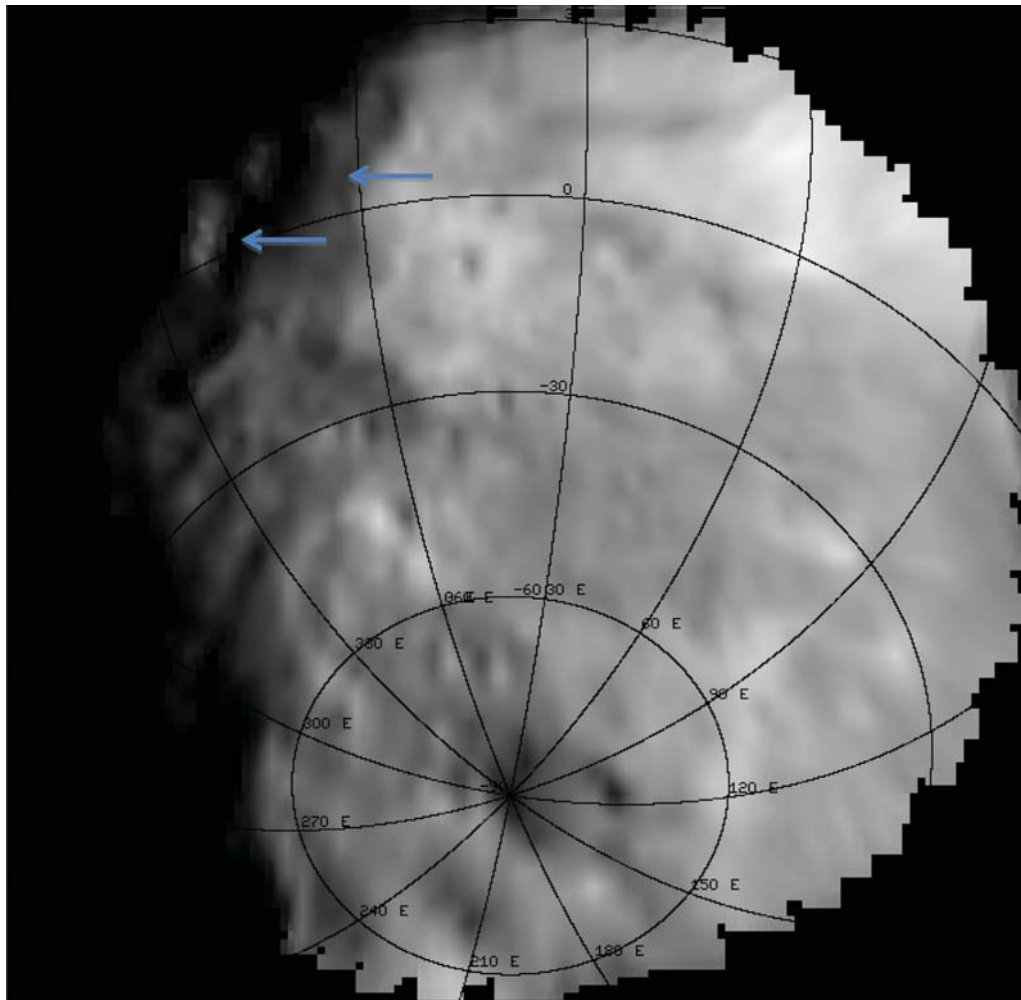


Fig. 3. Framing Camera RC1 image f2_362695687 with an arbitrary set of longitudes overlaid. Misidentified in the RC-based map as a crater rim (upper arrow) and peak (lower arrow) are the eastern and western rims, respectively, of the craters Marcia, Calpurnia and Minucia.

The geologic map in Fig. 2 was used to assist the team in highlighting and preparing for the types of features and terrains that would be encountered as the mission progressed. Outstanding issues to be addressed included: understanding the unique nature of Rheasilvia (whether there was a large extent of impact melt; why there was a central mound rather than a peak or an inner/outer ring complex); the processes that formed the ridge–trough complex; confirming circular features as impact craters and thus beginning to deconvolve the cratering history and relative age of the surface; clarifying the scale and extent of features so they could be compared to similar features on other bodies; and characterizing the nature of the higher- and lower-albedo regions, especially in relation to topography. The data also confirmed some important previous observations, including the presence of the large south-polar impact structure (Thomas et al., 1997a, b).

4.1.2. Survey iteration

The geologic map resulting from Survey data is shown in Fig. 4. For this second iteration, all basemap products were created using a coordinate scheme developed by the science team (known informally as the “Claudia” system after a crater at 0° longitude).

Our goal at this point was to facilitate the mapping process, which was most easily done by using the products created by team members assigned to that work. We thus used this team-derived coordinate system as shown in Figs. 4–22. Note that at the time of this writing, the PDS is providing Dawn data in a longitude system that can be obtained from the Claudia longitude by subtracting 150°.

FC continued to be the basemap, but improved color coverage and preliminary VIR data were also available. Though the interpretation of VIR band combinations is not clear as of this writing, we include the data because it informed some boundaries and interpretations. The geologic map was compiled in ArcGIS software (v. 10.1) using digital mapping techniques as outlined in the NASA Planetary Geologic Mapping Handbook (Tanaka et al., 2010). We chose to utilize ArcGIS instead of continuing to use Adobe Illustrator because digital mapping facilitates unit characterizations, feature correlation, and crater counts. This iteration of the map was produced at 1:1,000,000 scale.

At this resolution and coverage, we were able to identify and describe the gross characteristics of many of the main geologic units on Vesta (cratered plains and cratered highlands; equatorial and northern trough terrains; equatorial cratered terrain; bright

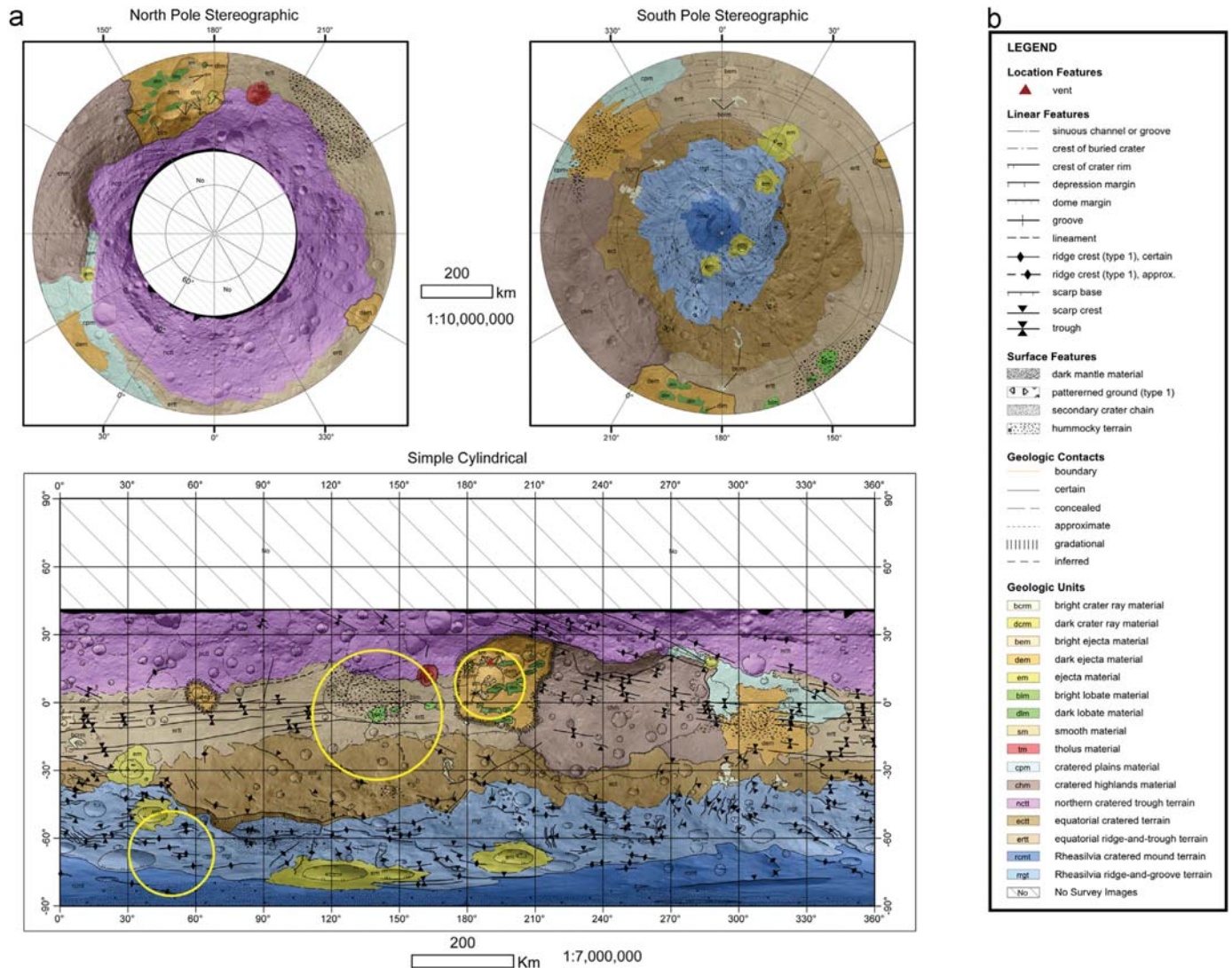


Fig. 4. Geologic map (a) and legend (b) based on Survey orbital data, produced at 1:1,000,000. Yellow circles indicate areas identified as having a diogenite (two small circles) or olivine (large circle) signature (Binzel et al., 1997). Note the locations of “orange”-toned surface material (stippled pattern) mapped as dark mantling material. This and all following figures show coordinates in the “Claudia” system utilized by the Dawn science team. (For interpretation of the references to color in this figure legend, the reader is referred to the web version of this article).

and dark ejecta and crater materials; and Rheasilvia mound and ridge-and-groove terrain). First estimates of crater size-frequency distribution were calculated based on those units (Marchi et al., 2012c; Schmedemann et al., 2012). We confirmed our observations from the previous iteration that no large melt sheet associated with Rheasilvia exists on the surface. Other crater features were identified and mapped with this iteration, including: craters with higher-albedo ejecta rays; craters with lower-albedo ejecta rays; and so-called “bimodal” craters with one rim portion sharp and the other more degraded (Krohn et al., 2012).

Major craters other than Rheasilvia were identified. The largest of these was the Veneneia impact structure, lying north of the younger Rheasilvia crater and identified by sections of rim scarp associated with a semi-circular topographic low. The interpretation of this set of features as an impact structure was vigorously debated among the mappers and the greater Dawn science team. Arguments against such an interpretation included: (a) the shape of the proposed impact structure was not circular and had an irregular vertical profile; (b) the center of the topographic low did not correspond precisely with the center of the proposed structure; and (c) the rim scarp was not continuous. The presence of Veneneia was not confirmed until the acquisition of HAMO data, which revealed that the rim scarp was more complete than had previously been believed.

The Saturnalia Fossae and Divalia Fossae were identified at this stage as continuous structural features rather than as scattered grooves or as disconnected peaks and valleys. These features' dimensions were mapped (northern cratered trough terrain and equatorial ridge and trough terrain respectively) and measured, and potential correlations with other terrains were assessed. Specifically, the two large ridge-and-trough complexes outside the south polar region were preliminarily associated with tectonic disruptions that occurred during the formation of Rheasilvia and Veneneia impact structures (equatorial and northern respectively) (Buczkowski et al., 2012; Jaumann et al., 2012).

Remaining issues at this stage of the iterative mapping process included clarifying the nature of the higher- and lower-albedo regions, and their relation to stratigraphy and topography.

4.1.3. HAMO iteration

For this iteration, shown in Fig. 5, we used a monochrome (clear filter) FC mosaic as our basemap. Images in this mosaic have an average spatial scale of ~ 70 m/pixel for HAMO. This base was imported into ArcGIS and supplemented by the Survey DTM. FC color ratio images from Survey orbit with a spatial scale of ~ 250 m/pixel and Visible and InfraRed (VIR; De Sanctis et al., 2011) hyperspectral images from the Survey and HAMO orbits with spatial scales of 700

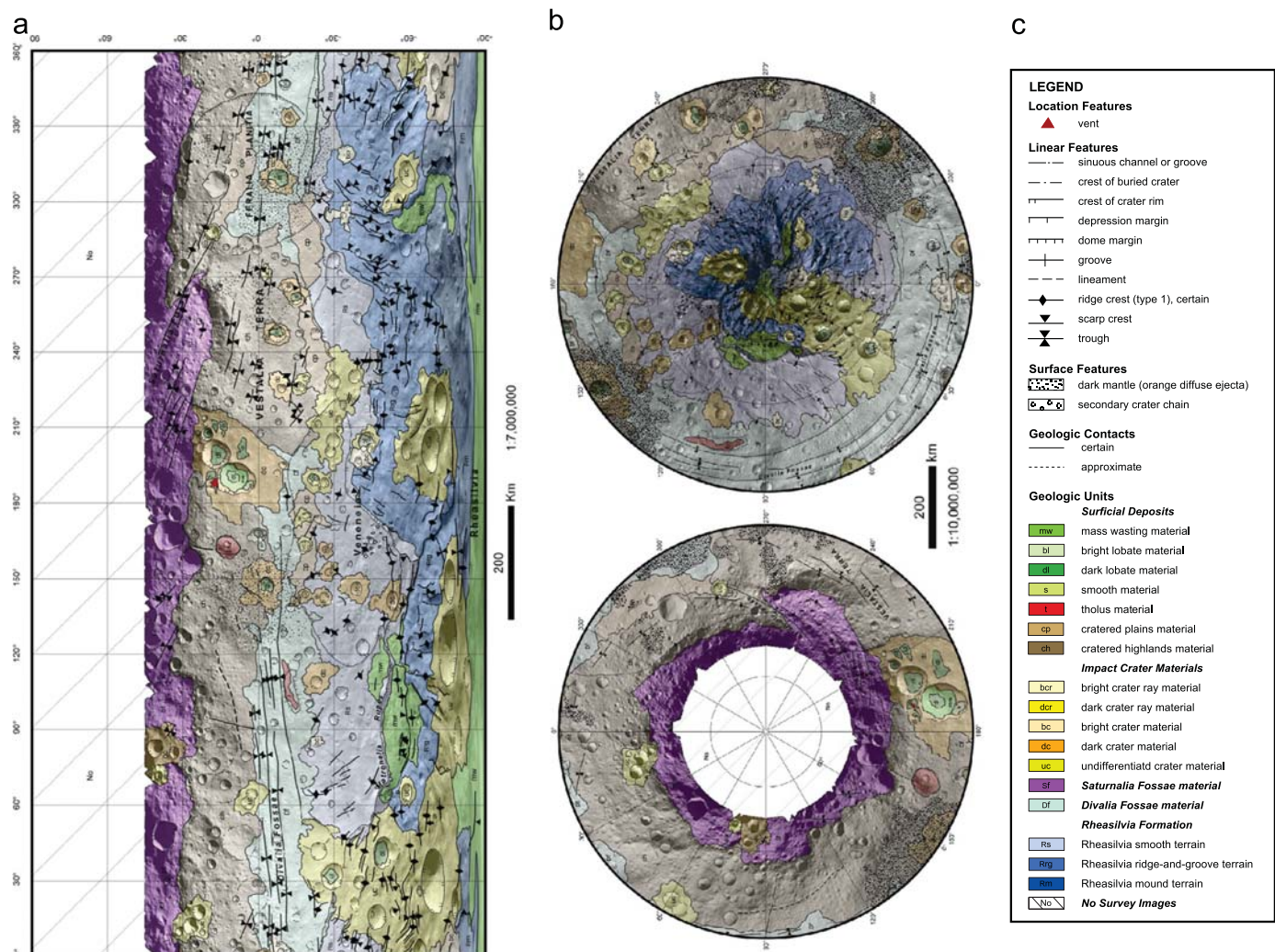


Fig. 5. Geologic map based on HAMO orbital data, as described in text. The map was produced at 1:500,000, using Framing Camera data as the basemap. Vesta is divided latitudinally into four areally extensive units: the Rheasilvia Formation, the Divalia Fossae and Saturnalia Fossae units, and cratered highlands. The blank area to the north represents regions for which there is no HAMO data. (a) Simple cylindrical projection; (b) North and South polar projections; and (c) legend.

and 200 m/pixel, respectively, provided information on surface composition and were used to refine unit boundaries. The final map in Fig. 5 was produced at a scale of 1:500,000.

In mapping this iteration, we expanded the list of units into a more traditional Description of Material Units (DOMU). Names were assigned to each unit, some associated with IAU-compliant names of the most prominent or characteristic feature associated with that unit (Roatsch et al., 2012).

With this iteration, the data was sufficient to resolve differences in surface texture down to the ~ 100 m scale, and a different illumination angle allowed albedo differences to be more clearly discerned through comparison to global Survey data. For this iteration, we mapped craters down to 2 km diameter at the request of the Dawn science team (for clarity, only craters > 6 km diameter are shown in Fig. 5). Using this information we were able to make several improvements to the geologic map, including (1) differentiating some larger units into smaller ones based on relative crater density and texture; (2) mapping the extent of Rheasilvia-modified terrain, which extends to nearly the equator in some places; (3) characterizing the extent of fine-textured ejecta materials at fresher craters; and (4) identifying and analyzing the characteristics of unique small-scale (tens of m) features such as units with lobate boundaries, and pitted terrain within crater floors. With regard to differentiation of larger units, we used improved surface texture information to divide portions of the Rheasilvia ridge-and-groove terrain (Fig. 4) into Rheasilvia smooth material (less-heavily cratered, smoother than surrounding Rheasilvia materials) and the more heavily cratered highlands and cratered plains north of it (Rs, cp and ch in Fig. 5 respectively). Units added included mass wasting material and Rheasilvia smooth material. We also revisited the boundaries of cratered terrain (cratered highlands and cratered plains in earlier maps) based on roughness of texture and relative crater density. Specifically, the area represented by cratered highlands increased at the expense of cratered plains. Additionally, the boundaries of the cratered highlands unit were expanded at the expense of ridge-and-trough terrain, to include areas with similar mean topography and FC color. The equatorial ridge-and-groove terrain and northern cratered trough terrain were renamed the Divalia Fossae ridge-and-trough and Saturnalia Fossae cratered trough units, as the improved resolution revealed that grooves (a more general term) were indeed troughs.

5. Material units

Based on data from the Dawn instruments, the surface of Vesta is comprised of four major terrains: individual craters and associated impact materials, widespread undifferentiated cratered units, the Saturnalia and Divalia Fossae units, and materials associated with the Rheasilvia impact structure. Other more localized units include lobate, smooth and tholus materials, and mass-wasting materials. We describe each of these units in terms of morphology, surface texture, relative crater density, topography and color ratio data. We also present type localities for each unit; images are from HAMO unless otherwise noted. The symbology and nomenclature used are shown in Fig. 5.

5.1. Surficial deposits

5.1.1. Mass wasting material (mw)

5.1.1.1. Description. This unit takes the form of deposits along the bases of steep slopes or crater walls due to mass movement of material, indicating the mobility of the regolith (Jaumann et al., 2012; Pieters et al., 2012). There are several morphologies represented within this unit. Slumps occur as sequences of

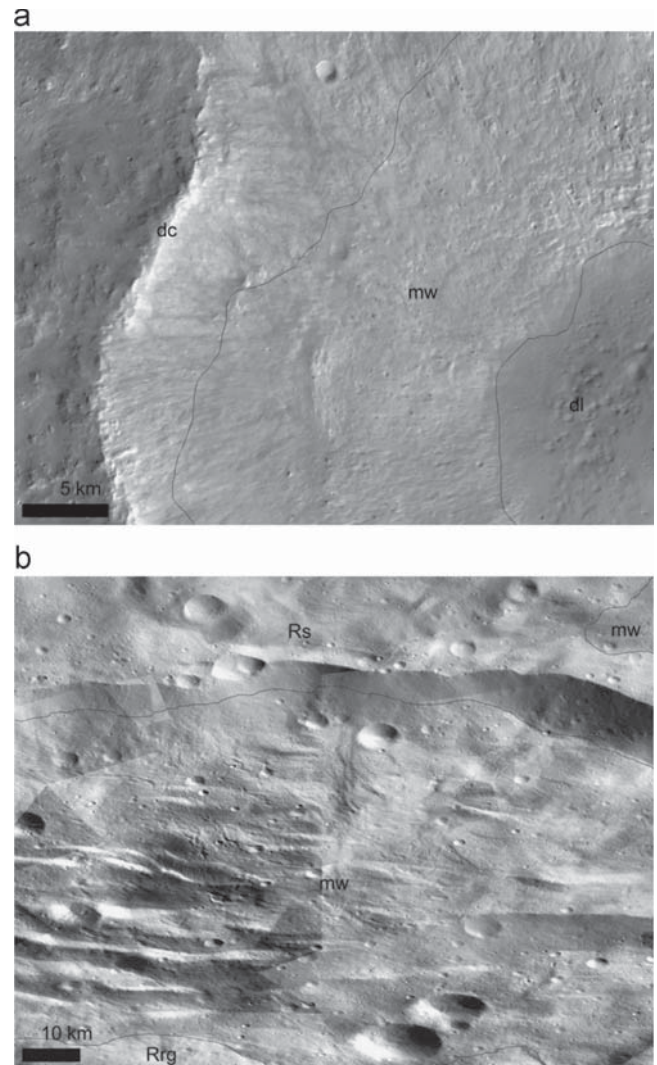


Fig. 6. Mass wasting material (mw). (a) Portion of a fan-shaped deposit in Marcia crater, with dark lobate material (dl) to the east in the crater floor. This deposit is characterized by subtle ridges of material radiating downslope. Note the individual boulders visible in the deposit. The center of this LAMO mosaic is at latitude 9.7° N, longitude 186.0° E in the Claudia coordinate system. North is up. (b) Slump deposit south of Matronalia Rupes that lies between Rheasilvia smooth terrain (Rs) and the Rheasilvia ridge-and-groove terrain (Rrg). Here, mw is comprised of subparallel blocks sliding downslope. The center of this LAMO mosaic is at latitude 54.5° S, longitude 91.9° E. LAMO mosaic. North is up. Image credit: NASA/JPL/DLR.

benches separated by crescent-shaped cliffs or scarps beginning at the top of a slope (Fig. 6a). Lobate or fan-shaped, smooth-textured deposits also occur, often associated with impact craters (Fig. 6b). More irregularly bounded deposits tend to have a hummocky texture and often display subtle or more diffuse boundaries.

5.1.1.2. Interpretation. We interpret this unit as debris falls, slumps or slides formed through slope failure that may be associated with a number of possible processes that involve mass movement of material downslope. Possible drivers include “seismic” shaking associated with impact crater formation or slope failure due to overburden. The team requested that these materials be mapped together by process rather than associated feature, in order to facilitate analysis of their distribution and thus how regolith mobility may vary by location.

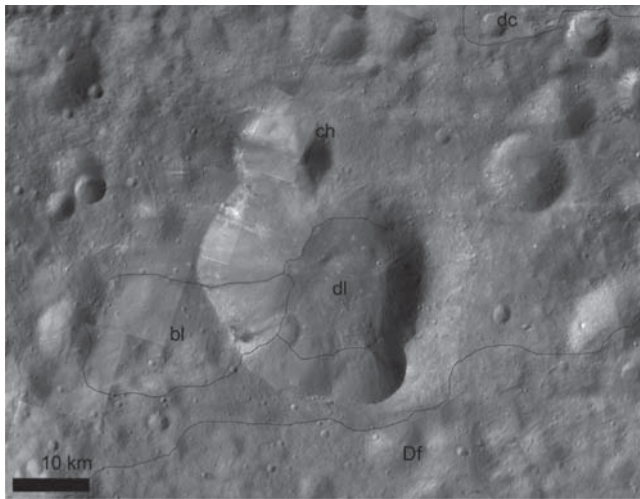


Fig. 7. Bright lobate material (bl). This type area lies south of Aricia Tholus. The bright lobate material is the smooth tongue of material draping the western rim of the crater. The center of this HAMO mosaic is at latitude 1.6°S, longitude 163.6°E. North is up. Image credit: NASA/JPL/DLR.

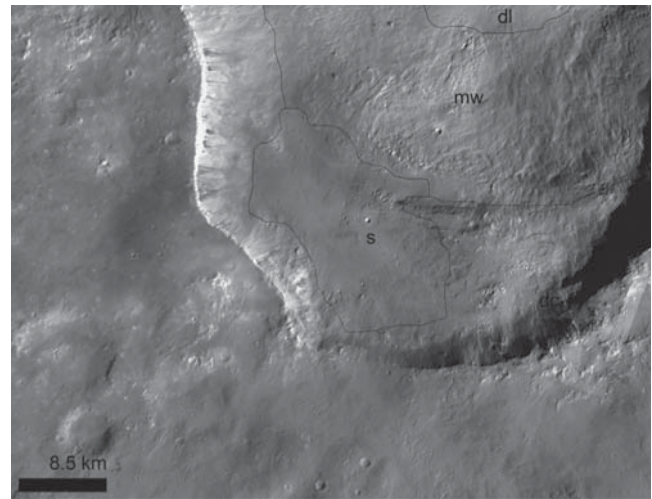


Fig. 9. Smooth material (s). This type area is in Marcia crater, lying on a southern bench between the rim and a mass wasting (mw) deposit downslope to the north. Note the difference in texture between smooth material and the more hummocky mw material. The center of this LAMO mosaic is at latitude 3.6°N, longitude 187°E. North is up. Image credit: NASA/JPL/DLR.

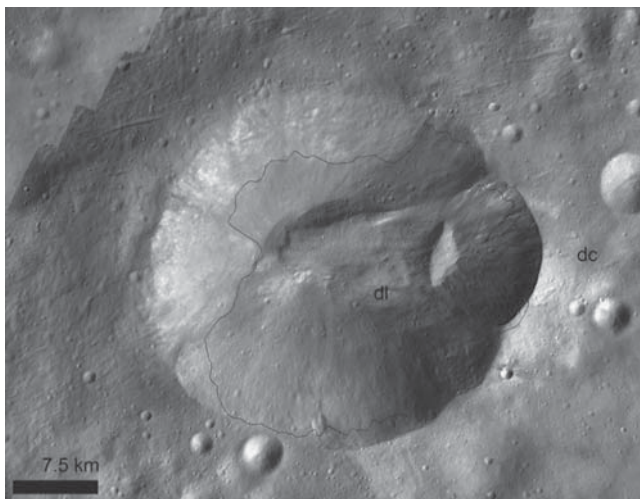


Fig. 8. Dark lobate material (dl). This type area lies in Octavia crater, within a patch of dark crater (dc) material. Here, dl appears fine-textured, with rolling topography. The center of this LAMO mosaic is at latitude 3.4°S, longitude 147.6°E. North is up. Image credit: NASA/JPL/DLR.

5.1.2. Bright lobate (bl)

5.1.2.1. Description. This unit is characterized by lobes that extend from crater rims or local topographic highs (e.g., scarps) onto crater floors or local topographic lows (e.g., Fig. 7). Deposits that fall within this unit have a convex-up topography, with lobate margins and smooth to hummocky surfaces. Deposits differ from mw deposits in their convex, positive topography and relatively sharp boundaries. Bright lobate deposits have intermediate albedo in FC monochrome images, with a yellow tone in color ratio images, though the color is not unique to this unit. These deposits generally have lower crater abundances compared to their surroundings.

5.1.2.2. Interpretation. We interpret the bright lobate unit to be impact-derived material, younger than the surrounding surface. These are likely flow deposits and may be the result of either impact ejecta flow lobes or impact debris transported downslope

as mass movement. Yellow areas in color ratio images tend to be smoother and may be composed of impact melts.

5.1.3. Dark lobate (dl)

5.1.3.1. Description. Dark lobate deposits (Fig. 8) are similar in morphology to the bright lobate unit but have a distinctively lower albedo. These materials extend from crater rims or scarps onto crater floors or local topographic lows. Deposits have a flat topography, with lobate margins and relatively smooth surfaces. Deposits differ from mw deposits in their flat surfaces, very smooth textures and relatively sharp boundaries. Dark lobate deposits have low albedo in FC monochrome images, with a yellow tone in color ratio images, though again, this color is not unique to this unit. These deposits generally have lower crater abundances compared to their surroundings.

5.1.3.2. Interpretation. Similarly to the bright lobate unit, we interpret the dark lobate unit to be impact-derived material; surface texture is consistent with impact melt (McCord et al., 2012; Reddy et al., 2012b).

5.1.4. Smooth unit (s)

5.1.4.1. Description. The smooth material unit is highly localized, consisting of several exposures found on the floor and rim of Marcia crater (Fig. 9). This unit displays overall smooth, dark and relatively featureless surfaces at the tens of meters scale, except for variable amounts of small impact craters and some clusters of pits. Smooth unit deposits have low albedo in FC monochrome images, and are typically blue–green to green–brown in FC color ratio images.

5.1.4.2. Interpretation. We interpret this smooth unit to be very young impact melt. Pit clusters are associated with low hydrogen and OH levels (De Sanctis et al., 2012; Prettyman et al., 2012) and have been interpreted as pits formed when volatiles from a volatile-rich impactor boiled off subsequent to crater formation (Denevi et al., 2012). Mapping results are consistent with this hypothesis. Alternately, the unit could be fine-grained materials deposited by mass movement.

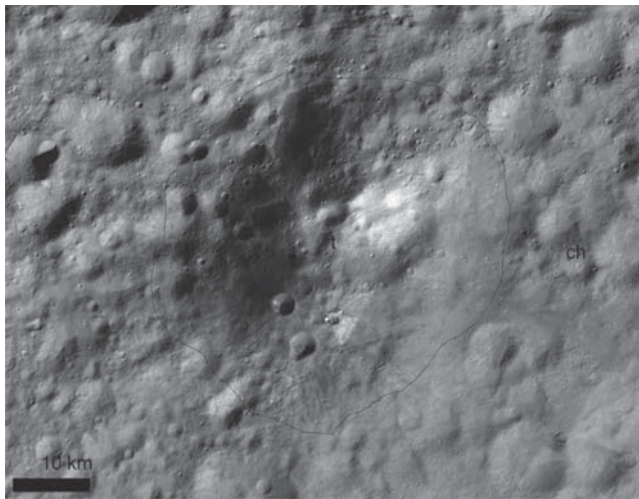


Fig. 10. Tholus material (t). This type area is Aricia Tholus. The tholus is cone-shaped, with a cratered surface; there is no indication of flows or other volcanic products associated with this structure. The center of this LAMO mosaic is at latitude 10°N, longitude 160°E. North is up. Image credit: NASA/JPL/DLR.

5.1.5. Tholus (t)

5.1.5.1. Description. There are two tholi mapped at this resolution: Aricia and Lucaria Tholi (Fig. 10). These are defined as isolated topographic highs with heavily-cratered surfaces and dark lobate patches associated with them. They have intermediate albedos in FC monochrome images and appear dark blue to purple in FC color ratio images.

5.1.5.2. Interpretation. We interpret the tholus unit to be impact-sculpted crust, possibly containing volcanic dikes or intrusions, or volcanic cones. Dark-rayed crater material and dark lobate patches on Aricia Tholus may indicate basaltic material exposed by impact cratering. Alternatively, the dark-rayed crater could have an exogenic source (i.e., carbonaceous meteorite), and the small lobate patches could be impact ejecta flows or impact melts (Reddy et al., 2012b).

5.2. Cratered terrains

5.2.1. Cratered highlands (ch)

5.2.1.1. Description. This extensive unit has a heavily-cratered surface and a higher albedo and overall topography than the surrounding plains (Fig. 11). The boundary between this and other units is occasionally subtle but discernable as a combination of steepening topographic slope and an increase in roughness of surface texture. This unit is concentrated along the equator and includes the Vestalia Terra high. An intermediate albedo is seen in monochrome FC images, with localized bright and dark patches. In FC color ratio images color ranges from purple-red to blue tones. Early analysis of VIR data led to an interpretation of the spectral signature of this unit as having howarditic mineralogy (De Sanctis et al., 2012).

5.2.1.2. Interpretation. We interpret this unit to be ancient terrain. The Vestalia Terra region may be a preserved section of ancient crustal materials (e.g., Raymond et al., 2013) or a mound of accumulated ejecta, modified by later impact cratering, producing a distinctive topographic high. Because the surface texture of cratered highlands is similar throughout, showing no distinct difference between the higher Vestalia Terra and the surrounding cratered

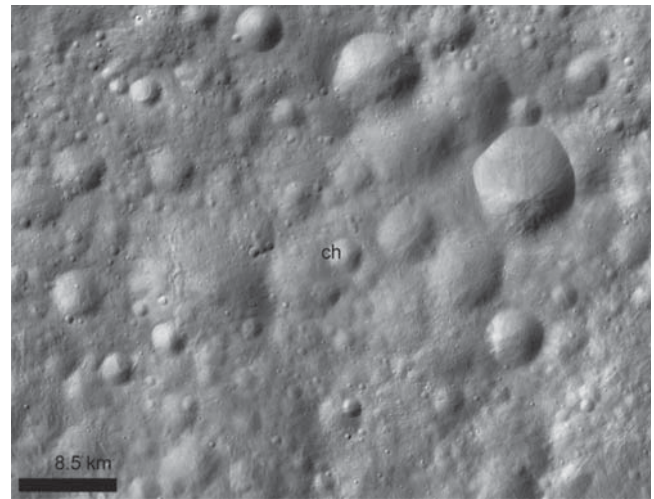


Fig. 11. Cratered highlands material (ch). The type area is northeast of Numisia crater. Note the abundance of overlapping craters of various sizes and states of degradation; many have subcircular, rather than circular perimeters. The center of this LAMO mosaic is at latitude 5.0°N, longitude 260.5°E. North is up. Image credit: NASA/JPL/DLR.

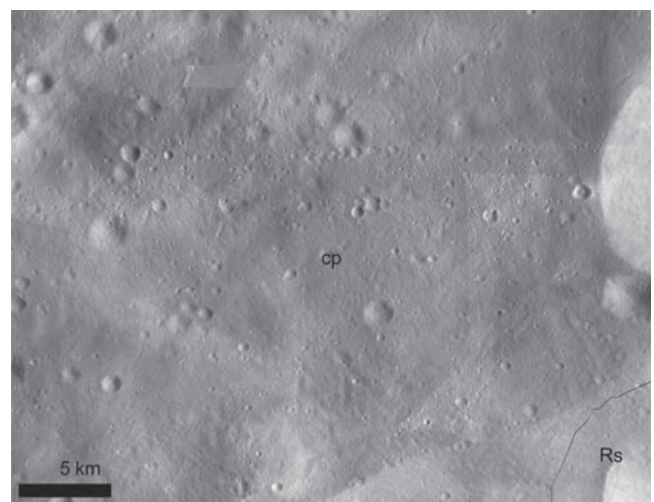


Fig. 12. Cratered plains material (cp). This type area is southwest of Drusilla crater. While many impact structures are present, the craters are smaller and fewer. The center of this LAMO mosaic is at latitude 23.5°S, longitude 239.5°E. North is up. Image credit: NASA/JPL/DLR.

highlands, the former interpretation is currently preferred. If this is the case, Vestalia Terra may be the oldest terrain on Vesta.

5.2.2. Cratered plains (cp)

5.2.2.1. Description. The cratered plains unit (Fig. 12) occurs as narrow, somewhat isolated regions of smoother, topographically lower, relatively sloping terrain with lower crater density than the Divalia Fossae unit. All occurrences of this unit are bounded by cratered highlands, the Divalia Fossae unit or both.

5.2.2.2. Interpretation. We interpret this unit to be ancient cratered terrain degraded or smoothed by either the emplacement of a thinning layer of Rheasilvia ejecta, or the degradation of sloping material over time.

5.3. Crater material

Impact cratering is an important geologic process on Vesta. Craters are also probes into previous geologic conditions because they excavate into lower layers. Crater morphology shows many similarities to other small, airless, rocky bodies. Small, fresh craters are characterized by sharp-crested, narrow rims and bowl shapes, while larger fresh craters have flat floors and may display slumping of rim walls, finer-textured floor fill, or visible ejecta material (craters 1–3 km in diameter are of indeterminate state of degradation because morphology is below resolution, and are mapped as points). Degraded craters have subdued but distinct, continuous rims and varying shapes. Enclosed sub-circular or ovoid depressions also exist; these have lower topography than the surroundings but lack a discernable rim or bowl shape. Complex craters are characterized by high-topography rugged hills and arcuate scarps forming partial rings. We interpret the state of degradation to be generally correlated with crater age, with the least degraded craters being the youngest and the most degraded being the oldest; however, differences in the rheology of target materials may affect the shape of the crater. Some sharp-rimmed craters show degraded rim sections (bi-modal craters). The process that forms such craters is unclear. One hypothesis is that such craters were formed on a slope, with the upslope side being more susceptible to mass-wasting (e.g., Krohn et al., 2012); many, but not all, such craters fit this model.

There are several types of crater materials that show unique features that provide clues to underlying layers. These are enumerated below.

5.3.1. Bright crater ray material (bcr)

5.3.1.1. Description. This material forms halos, streaks or patches radiating from relatively fresh impact craters, extending to or beyond one crater diameter (Fig. 13). These rays are very thin, as the underlying topography, and in some cases, the underlying texture, are visible. Additionally, opacity decreases with increasing distance from the source. Bright crater ray material displays high albedo in monochrome FC images, and a bright white to yellow color in FC color ratio images.

5.3.1.2. Interpretation. We interpret this high albedo material to be mantling impact ejecta excavated from deeper layers, analogous to

lunar crater rays. Lunar rays are considered the youngest features on the Moon (e.g., Dietz, 1946); we infer from superposition relationships (rays are stratigraphically the highest feature) that bright crater rays are relatively young features on Vesta, not yet affected by space weathering (Pieters et al., 2012).

5.3.2. Dark crater ray material (dcr)

5.3.2.1. Description. Dark crater ray material (Fig. 14) forms low-albedo radial halos, streaks or patches that mantle underlying material and extend to or beyond one crater diameter. Rays often are associated with craters in which thin (100–500 m thick), discrete layers of dark material are visible in the crater walls; craters that have dark crater ray material often occur in clusters. The distribution of these rays around craters is often asymmetrical and the underlying topography and texture are visible. Opacity decreases with increasing distance from the source. Dark crater rays display low albedo in monochrome FC images and a dark purple color in Clementine-type FC color ratio images.

5.3.2.2. Interpretation. We interpret this low albedo ray material to be impact ejecta excavated from thin, dark, discontinuous subsurface layers whose boundaries can be inferred by the presence of these dark crater rays; alternatively, rays could consist of low albedo material dispersed from dark, possibly carbonaceous impactors. We infer from superposition relationships that dark crater rays are relatively young features.

5.3.3. Bright crater material (bc)

5.3.3.1. Description. Bright crater material (Fig. 15) is characterized by a continuous, high-albedo ejecta blanket, and pronounced continuous crater rims elevated relative to surrounding materials.

5.3.3.2. Interpretation. We interpret bright crater material to be high-albedo, relatively fresh and unmodified crater deposits – including rim, ejecta and some floor materials – emplaced by impact processes.

5.3.4. Dark crater material (dc)

5.3.4.1. Description. Dark crater material is present as continuous, very low albedo ejecta blankets associated with pronounced continuous crater rims elevated relative to surrounding materials

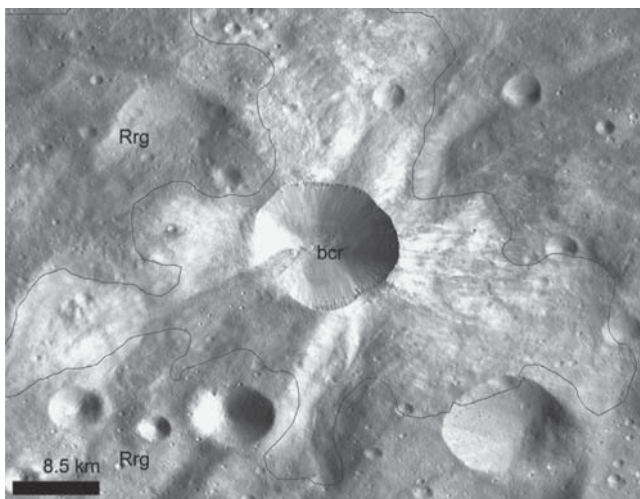


Fig. 13. Bright crater ray material (bcr). This type area is at Canuleia crater, which formed in Rheasilvia ridge-and-groove (Rrg) terrain. Note the light-toned streaks radiating from the crater are not uniform; this is common for bcr material. The center of this LAMO mosaic is at latitude 33.8°S, longitude 294.5°E. North is up. Image credit: NASA/JPL/DLR.

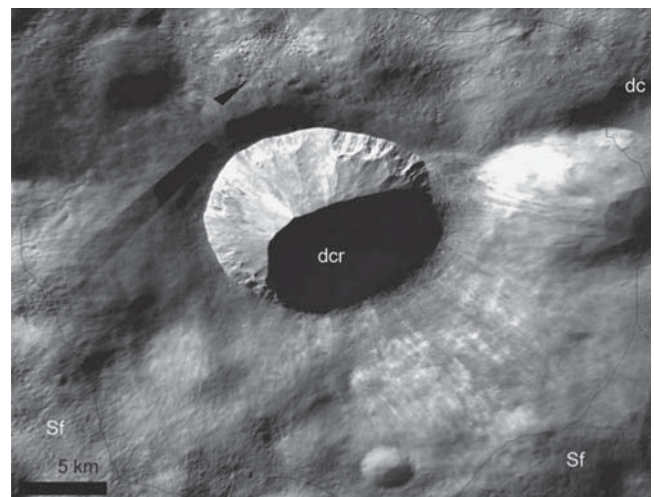


Fig. 14. Dark crater ray material (dcr). This type area is at Arruntia crater, within the Saturnalia Fossae unit (Sf). Discontinuous dark-toned streaks radiate from the crater. Here, the low sun angle reveals the rough, mesh-like texture of Sf, which is mantled by dcr. The center of this LAMO mosaic is at latitude 39.0°N, longitude 75.2°E. North is up. Image credit: NASA/JPL/DLR.

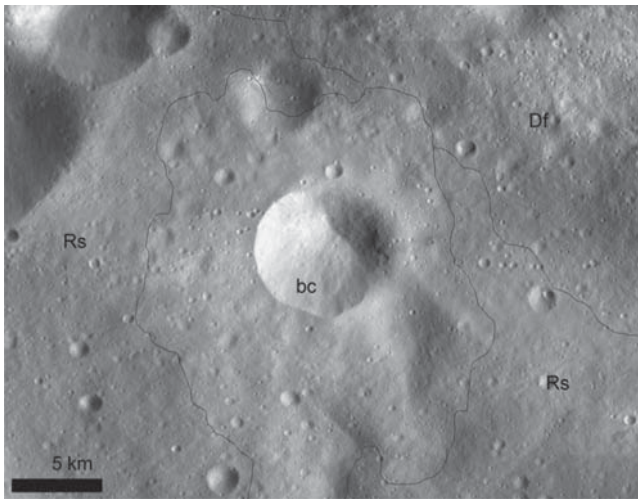


Fig. 15. Bright crater material (bc). This type area is southwest of Lucaria Tholus, at a junction between the Rheasilvia smooth terrain (Rs) and the Divalia Fossae unit (Df). The texture is similar to that of the Rs terrain, but is slightly rougher and lighter-toned. The center of this LAMO mosaic is at latitude 22.7°S, longitude 85.2°E. North is up. Image credit: NASA/JPL/DLR.

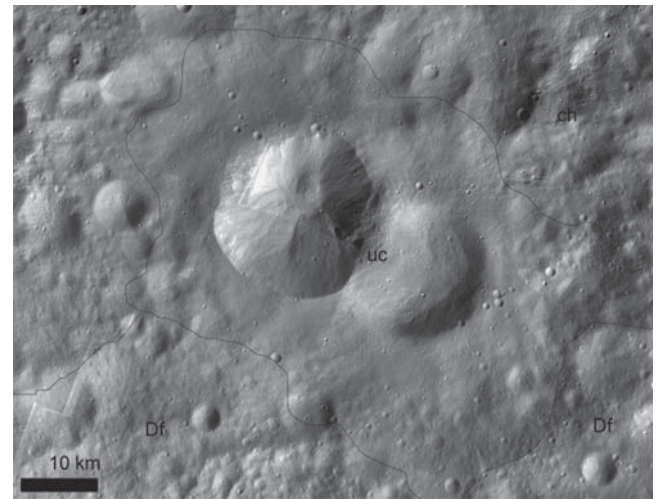


Fig. 17. Undifferentiated ejecta material (uc). Here uc material lies near Gegania crater, in the Divalia Fossae unit (Df). The texture is smoother than the surrounding unit but otherwise morphologically similar. The center of this LAMO mosaic is at latitude 3.1°N, longitude 63.1°E. North is up. Image credit: NASA/JPL/DLR.

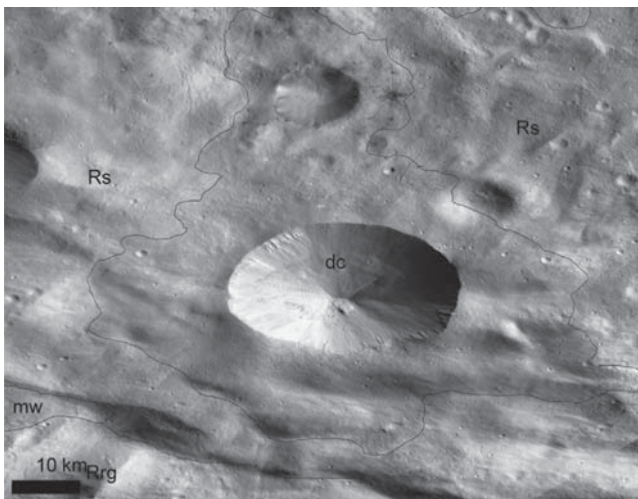


Fig. 16. Dark crater material (dc). This type area is south of Laelia crater, which formed in Rheasilvia smooth terrain (Rs). Note the similarity in texture to bc, but darker-toned than the surrounding Rs unit. The center of this LAMO mosaic is at latitude 51.3°S, longitude 140.7°E. North is up. Image credit: NASA/JPL/DLR.

(Fig. 16). Most parent craters display dark layers exposed in their interior walls.

5.3.4.2. Interpretation. We interpret dark crater material to be similar to craters with dark crater ray materials, where ejecta is inferred to be excavated from dark, discontinuous subsurface layers.

5.3.5. Undifferentiated ejecta material (uc)

5.3.5.1. Description. Ejecta material that is continuous and relatively smooth, but has no other discriminating characteristics or clear stratigraphic placement (Fig. 17), is mapped as ejecta material, undifferentiated. Pronounced continuous crater rims elevated relative to surrounding materials tend to be associated with such ejecta deposits. Some deposits display a more distinctive color (in the FC color ratio mosaic) compared to underlying terrain; specifically,

colors in between those of the bright ejecta (yellows to yellow-green) and dark ejecta (dark violet), thus violet-red to green-blue.

5.3.5.2. Interpretation. We interpret this material to be relatively fresh and unmodified, well-preserved impact crater deposits.

5.4. Ridge-and-trough terrain

Linear structural features were discovered on the Martian moon Phobos decades ago in Viking orbiter imagery; [Thomas and Veverka \(1979\)](#) suggested that these grooves were most likely the result of the large impact that formed Stickney crater. Furthermore, they predicted that similar lineaments would be observed on other cratered bodies, since craters formed in the laboratory (e.g., [Fujiwara and Asada, 1983](#)) and on planets (e.g., [Reimold et al., 1998](#)) tend to display radial fractures. This prediction was realized when images of asteroids began to be returned to Earth. A number of different types of linear structural features – including grooves, fractures, troughs and ridges – have been observed on a number of asteroids, including Gaspra ([Veverka et al., 1994](#)), Ida ([Sullivan et al., 1996](#)), Itokawa ([Sasaki, 2006](#)), Eros ([Prockter et al., 2002](#); [Buczkowski et al., 2008](#)), Steins ([Keller et al., 2010](#)), Lutetia ([Sierks et al., 2011](#); [Thomas et al., 2012](#)) and now Vesta ([Jaumann et al., 2012](#); [Buczkowski et al., 2012](#)).

While the ridges and troughs that characterize these terrains are likely the result of intense faulting of pre-existing terrain, we mapped the material as separate units because the crust has been disrupted to such an extent that it is impossible to identify the characteristics of the pre-existing terrain, to classify it.

5.4.1. Saturnalia Fossae material (Sf)

5.4.1.1. Description. The Saturnalia Fossae unit is found in the northern hemisphere. Topographically lower than surrounding units, the unit consists of heavily-cratered terrain cross-cut by NW-SE trending degraded ridges and flat-floored troughs. The largest, most prominent of these troughs is Saturnalia Fossa, at widths up to 39.2 km, depths up to 4.0 km and a length of at least 458 km; a trough to the south of Lepida crater is potentially a continuation of the fossa ([Buczkowski et al., 2012](#)), which could mean its length is as great as 640 km. This potential continuation is much deeper than the average fossae (~6 km), perhaps due to

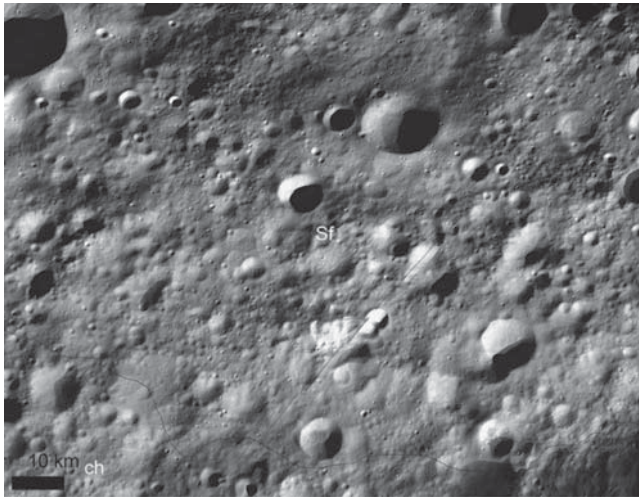


Fig. 18. Saturnalia Fossae material (Sf). This type area lies west of Scantia crater, along a group of ridges. Note the high crater density and the surface texture, which appears more rough than the Divalia Fossae unit, but this may simply be a question of the illumination being more conducive to revealing roughness. The center of this LAMO mosaic is at latitude 33.1°N, longitude 236.3°E. North is up. Image credit: NASA/JPL/DLR.

reactivation during the Rheasilvia impact. Associated troughs have widths that range from ~5 to ~15 km, lengths of ~20 to ~140 km, and depths of 50 m to ~2.0 km. The fossae cut terrain containing the highest crater density observed on Vesta (e.g., Fig. 18). The unit is intermediate albedo in FC monochrome images, and blue-purple in FC color ratio images.

5.4.1.2. Interpretation. We interpret the Saturnalia Fossae unit to be Vestan crustal material, modified into fault-bounded graben by impact and tectonic processes (Buczkowski et al., 2012). Fault-plane analysis suggests that northern troughs and grooves of the Saturnalia Fossae may be some form of tectonic response to formation of the Veneneia impact structure (pre-Rheasilvia). This unit represents one of the oldest on Vesta.

5.4.2. Divalia Fossae material (Df)

5.4.2.1. Description. The Divalia Fossae unit is characterized by terrain cut by prominent ridges and deep, flat-floored troughs trending parallel to the equator (Fig. 19). Trough widths range from 10 to 22 km, lengths are 90–465 km, and depths are 1–2 km; the largest is Divalia Fossa, at ~465 km length and width ranging from 14.5 to 21.8 km. Numerous craters superpose the troughs. This unit does not have a unique color in FC monochrome or color ratio images. It displays intermediate crater density, and is stratigraphically younger than the Rheasilvia Formation and Saturnalia Fossae unit.

5.4.2.2. Interpretation. Like the Saturnalia Fossae unit, we interpret the Divalia Fossae unit to consist of Vestan crustal material, heavily modified into fault-bounded graben by impact and tectonic processes. In the case of the Divalia Fossae, formation of this sequence of ridges and troughs (Buczkowski et al., 2012; Jaumann et al., 2012) is consistent with interpretation that they formed by tectonic response to formation of the Rheasilvia impact crater.

5.5. Rheasilvia formation

5.5.1. Rheasilvia smooth terrain (Rs)

5.5.1.1. Description. Much of the outer boundary of the Rheasilvia impact crater is defined by Rheasilvia smooth terrain (Fig. 20). This

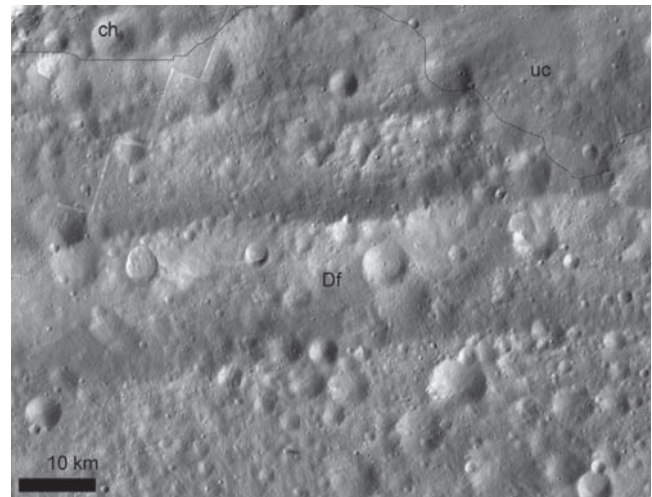


Fig. 19. Divalia Fossae material (Df). This type area is south of Gegania crater, just south of the cratered highlands (ch) and intersected by a deposit of crater ejecta, undifferentiated (uc). Here, Df displays subparallel ridges, less heavily cratered than the ch deposit to the north. The center of this LAMO mosaic is at latitude 9.6°S, longitude 61.4°E. North is up. Image credit: NASA/JPL/DLR.

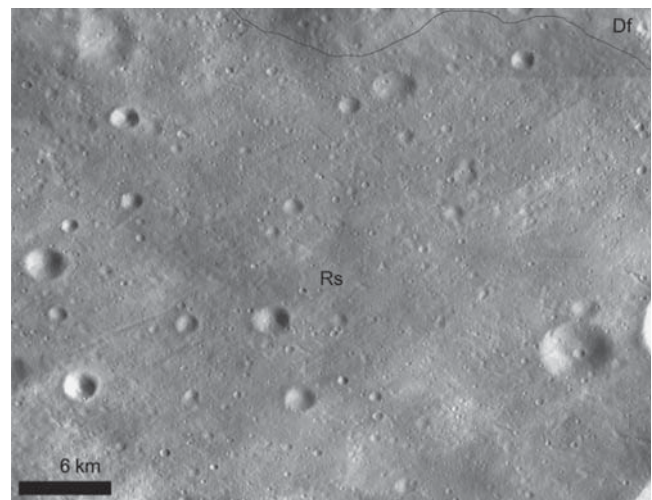


Fig. 20. Rheasilvia smooth material (Rs). This type area lies west of Pinaria crater south of the Divalia Fossae unit. Note the smooth topography, flatter and less cratered than Df. This LAMO mosaic is centered at latitude 30°S, longitude 354°E. North is up. Image credit: NASA/JPL/DLR.

unit occurs as irregularly-bounded regions of very smooth material at lower resolution, often located on slopes or topographically lower regions. This unit has a slightly lower albedo than the cratered plains and the Divalia Fossae unit to the north. Crater density is moderate; clusters of dark-rayed craters often occur within the confines of this unit.

5.5.1.2. Interpretation. We interpret this smooth member to be ejecta emplaced during the Rheasilvia impact event, potentially modified later through mass movement of material.

5.5.2. Rheasilvia ridge-and-groove terrain (Rrg)

5.5.2.1. Description. The Rheasilvia floor is characterized by curvilinear ridges and grooves that are kilometers to tens-of-kilometer long (Fig. 21). There are two pronounced trends: one running sub-radially from the Rheasilvia central mound, and one

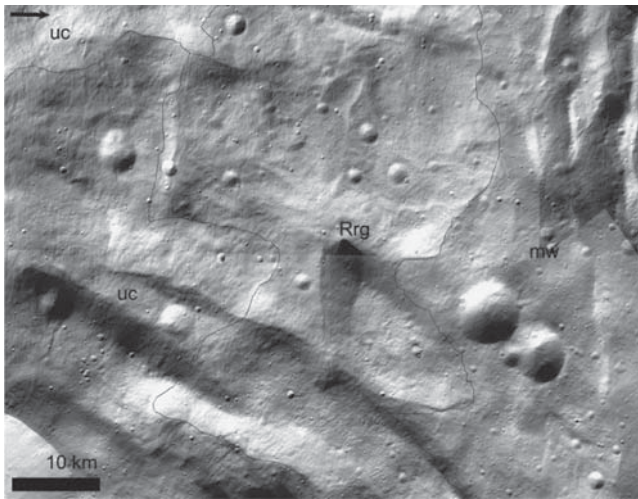


Fig. 21. Rheasilvia ridge-and-groove material (Rrg). This type area lies northwest of Severina crater. Here, radial grooves and ridges curve between deposits of uc (south) and mw (north). The center of this south polar projection LAMO mosaic is at latitude 67°S, longitude 88.7°E. Arrow indicates direction of true north. Image credit: NASA/JPL/DLR.

paralleling the curvilinear scarps that bound Rheasilvia. Lobate deposits appear downslope of some steep sloped ridges and mantle underlying cratered terrain. Crater density appears lower than Vestalia Terra, Divalia Fossae, and Saturnalia Fossae. Rheasilvia Formation ridge-and-trough terrain appears blue–green in FC color ratio images.

5.5.2.2. Interpretation. We interpret this member to be Rheasilvia material, heavily modified by post-impact processes. Impact materials form the floor of the Rheasilvia impact structure and are derived from the Rheasilvia impact event (Schenk et al., 2012). It is not clear how much of these impact materials are comprised of actual impact melt. Lobate deposits along steep scarps and ridges are interpreted to be slump or other mass wasting deposits, driven by overburden.

5.5.3. Rheasilvia mound terrain (Rm)

5.5.3.1. Description. The center of Rheasilvia is characterized by an irregular topographic high bisected by a discontinuous scarp. This central mound (Fig. 22) has a relatively low crater density between 90 and 180° longitude; crater density is higher elsewhere. The surface is granular-textured and smoother than the crater floor. In several areas pre-existing topography can be seen as rugged ridges surrounded by younger surface materials. These ridges appear to be aligned with the larger trending ridges and grooves. Shallow lineaments on the surface mirror this trend across the mound. Lobate deposits (mw) occur along the base of the scarp.

5.5.3.2. Interpretation. We interpret this member to be comprised of materials that form the broad central peak of Rheasilvia. Central peaks form by the rebound of the impact point, excavating rocks from depth; the composition of the mound may thus be a probe into the composition of the Vestan subsurface. The scarp boundary appears unstable, as evidenced by the presence of mw deposits. Crater density is interpreted to be lower because craters have been degraded, obscured or destroyed by slope failure. Smaller ridges surrounded by younger surface materials are interpreted to be extensions of the Rheasilvia ridge-and-groove member (Rrg) partially buried and subdued by mw material.

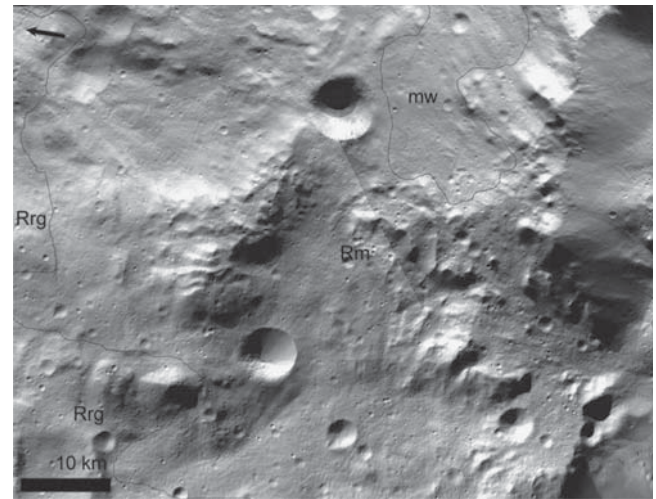


Fig. 22. Rheasilvia mound material (Rm). This type area is west of Severina crater. The unit is hummocky, with mw material commonly lying within low regions. In this case, a tongue of mw occurs to the east between a crater and a rugged ridge. The center of this south polar projection LAMO mosaic lies at latitude 74.7°S, longitude 279°E. Arrow indicates direction of true north. Image credit: NASA/JPL/DLR.

5.6. Surface features

Vesta has distinctive features that overlie several of the geologic units noted here. These features differ from the geologic units defined above because they mantle but do not cross-cut, deform, or otherwise alter the underlying units. Such features are shown as symbols on the map.

5.6.1. Dark mantling material

This feature is diffuse ejecta material of a unique spectral signature, mantling underlying topography. This material is localized in several patches, the largest of which is the type feature associated with the Oppia crater ejecta blanket. This feature is visible as a low albedo mantle in monochrome images, more clearly identified as brown-toned in FC “true” color images, and orange-toned in FC stretched color images. It is potentially correlated with a 2.8 μm feature in VIR data (De Sanctis et al., 2012). Like most ejecta, this feature displays decreasing opacity with increasing distance from the source. The mantle is continuous and has thickness, and we have therefore mapped it as a unit, though it clearly “mantles” material lying below it. We interpret this feature to be diffuse impact ejecta of unique composition or physical properties, potentially excavating a layer of distinctive mineralogy or lithology.

5.6.2. Catena

Catena appear as linear, overlapping or chevron-shaped clusters of similar diameter craters. We interpret catena to be chains of secondary craters associated with the formation of a larger impact crater.

6. Relative stratigraphy

We used superposition relationships, crater frequency, and cross-cutting relationships to determine a preliminary stratigraphic sequence for Vesta. The oldest coherent unit is cratered highlands material, a unit that includes the high-standing Vestalia Terra. This unit is the lowest stratigraphic unit and is the best candidate for representing Vesta’s ancient, primary crust, if it still exists. Stereo

topography (Preusker et al., in preparation) and geophysical data (Raymond et al., 2013) suggests that Vestalia Terra is not only a topographic high but also has both a positive gravity and density anomaly, suggesting it is a remnant of Vesta's original crust.

Cratered plains have fewer craters, a smoother texture, and are lower topographically, than cratered highlands. They are thus interpreted to have formed later. It is currently not clear whether the few troughs within the cratered plains are associated with Divalia Fossae or the Rheasilvia Formation, or formed by other processes; nor is it entirely clear whether they cross-cut this unit, or are truncated by it. Unlike the cratered highlands, cratered plains' smoother texture may indicate mantling by some ejecta from the Rheasilvia impact. An alternate interpretation for this smoother texture is that because these isolated "islands" are on downsloping terrain, the terrain has been smoothed through slumping or degradation through mass movement.

The Saturnalia Fossae unit cross-cuts the cratered highlands and plains and thus must post-date these units, but is cross-cut by the Divalia Fossae unit and is therefore stratigraphically older than that unit. The poles of the planes described by the graben in this unit are oriented around a point that describes the central floor of Veneneia, indicating that the Saturnalia Fossae were formed through fracturing associated with the Veneneia impact (Buczkowski et al., 2012; Jaumann et al., 2012).

The Rheasilvia Formation cross-cuts (in the case of the ridges and grooves) or stratigraphically superposes (in the case of ejecta material), cratered highlands and plains. While the extent of the units in this formation do not reach far enough north to reveal a stratigraphic relationship between it and the Saturnalia Fossae unit, because the Rheasilvia Formation cuts (Rrg) or overlies (Rs) the cratered plains and highlands, but is cut by Divalia Fossae, it must lie stratigraphically between these units. We note also that if the formation of Veneneia drove the fracturing associated with the Saturnalia Fossae, and is overlain by Rheasilvia, then Rheasilvia must post-date the Saturnalia Fossae. The Rheasilvia Formation itself overprinted or obliterated any visible vestige of older units.

The Divalia Fossae unit cross-cuts all lower units, except possibly the cratered plains, as noted above. As is the case for Veneneia, the poles of the planes described by the graben in this unit are oriented around a point that describes the central floor of Rheasilvia. This indicates that the unit is the result of tectonic deformation associated with the Rheasilvia impact (e.g., Buczkowski et al., 2012; Jutzi and Asphaug, 2011). An alternate hypothesis is that troughs formed due to spin up of Vesta, although the spin up would still be due to the impact.

Craters exist at each stratigraphic level; some, such as Marcia, dominate the pre-existing terrain to a great extent. Marcia Crater is a special case, in which the ejecta is unique and the craters themselves overlie all other units except for the ones internal to them (mw, t, dl). Marcia is the youngest large (> 25 km) crater on the surface of Vesta, with cratering model age estimates of ~40–160 Ma (Williams et al., in preparation). As noted above, craters are mapped and placed stratigraphically based on the level of degradation of rims, as well as infill and slumping. Sharp craters are interpreted to be the youngest craters, while degraded and highly degraded craters and depressions are considered progressively older. Based on inference from the lunar example, we also interpret rayed craters to be very young. Because craters with softened and slightly more subdued morphology than the freshest craters do not have ray systems, either bright or dark, this indicates that surface soil is being altered and such features are being erased over time (Pieters et al., 2012). Dark-rayed craters lie stratigraphically above the Divalia Fossae unit, but because they tend to cluster in discrete locations and excavate a narrow, low-albedo stratigraphic layer, these crater rays are interpreted to be due to excavation of this dark layer rather than an indicator of age.

Again, because these craters do not occur globally, it is not clear where this class of craters lies within the stratigraphic column.

The many relatively young surficial deposits indicate that portions of Vesta's crust have been eroded or altered more recently. Many of these deposits are associated with specific young craters (e.g. the lobate material, pitted terrain, mass movement in and around Marcia) and the driving force behind their formation is likely associated with the crater. For example, pitted terrain has been hypothesized to have formed through volatile release associated with crater formation (Denevi et al., 2012), while mass movement of material in many cases is likely due to slumping from crater formation or oversteepening. Other mass movement deposits are likely also associated with slumping of oversteepened scarps or other high points. Mass movement events are most likely driven by the seismic shock created by nearby small impacts.

The youngest features on Vesta are those mapped surface features where the underlying geologic unit is still visible. The most prominent of these is the dark mantle feature. This feature is of uncertain composition, but its broad extent in several locations suggests the presence of a layer of unique composition that has been excavated in these locations. The presence of this feature is not correlated with topography: Oppia lies at a topographic low, for example, and Vestalia Terra is the highest point on Vesta. There is, however, a correlation with latitude. All craters excavating dark mantling features occur between 30° and 0° latitude; none exist within the Rheasilvia Formation. The inference is that either the excavated layer associated with the dark mantling feature was present but was stripped by the Rheasilvia impact, or the layer was never present south of the equator. Alternatively, the source of the material may be exogenic (the impactors) rather than endogenic (Vesta's crust).

Volcanic materials were predicted to occur on Vesta's surface, based on telescopic spectral evidence of basaltic mineralogies, and the presence of basaltic minerals and glassy textures that are diagnostic of terrestrial basaltic lava flows found in the HED meteorites (e.g., Binzel et al., 1997; Gaffey, 1997; McCord et al., 1970; McSween et al., 2011). Wilson and Keil (1997, 1996) used mathematic and petrologic models to predict the types of volcanic deposits that should occur on Vesta, including surface lava flows a few kilometers to several tens of kilometers in length, channelized flows on steeper slopes, a lack of uniform sheet flows and shield volcanoes, shallow dikes and deep intrusions, and minimal pyroclastic fall deposits. These studies suggested that volcanic features, particularly lobate lava flows, might be resolved on Vesta's surface by Dawn, although such deposits likely would have been heavily disrupted by impact craters and thus not easily recognized. Analysis of HAMO and LAMO images covering ~85% of Vesta's surface has revealed no unequivocal morphological evidence for volcanic-related flow features on the surface. The lack of discrete volcanic features on Vesta is consistent with the hypothesis, based on analysis of basaltic material in the HED suite, that volcanism on Vesta occurred only during the first ~10–100 Ma of Vesta's history (e.g., McSween et al., 2011; Schiller et al., 2010), and that since then impact processes have degraded any ancient volcanic features to the point where they cannot be distinguished.

7. Absolute age-dating based on crater statistics

Crater counting is a common technique used to derive relative and absolute ages for planetary surfaces, based on the principle that the older a surface is, the more craters it accumulates from impacts (Hartmann, 1966a,b; Hartmann and Neukum, 2001). We have not used crater statistics for unit dating; our units are based solely on traditional geologic mapping principles such as cross-cutting

relationships. Rather, we present here initial crater statistics that have been derived from the units mapped.

In the case of Vesta, counts have been conducted using different methodologies for counting and for determining absolute ages from those counts (e.g., Marchi et al., in this issue; O'Brien et al., in this issue; Schmedemann et al., in this issue). We note that there is not full consensus on which units can be reliably assessed for absolute age through crater counting statistics using HAMO data. Those units that most workers agree can be reliably dated using larger (> 10 km diameter) craters fully resolvable by HAMO include cratered highlands (ch), Rheasilvia ridge-and-groove terrain and Rheasilvia smooth terrain (Rrg and Rs, part of the Rheasilvia Formation), and the Divalia Fossae and Saturnalia Fossae units (Df and Sf), both categorized as ridge-and-trough material. A detailed treatment of absolute age-dating of the surface of Vesta based on crater statistics can be found in Marchi et al. (in this issue), O'Brien et al. (in this issue) and Schmedemann et al. (in this issue).

In each method, the diameter of every crater ≥ 10 km (≥ 2 km for this work) for each geologic unit was measured and recorded using ArcGIS tools (e.g., Kneissl et al., 2011), using the HAMO and LAMO clear filter FC mosaics as a base, along with elevation data from the Gaskell shape model to assist in crater identification.

7.1. Method 1

In the method utilized by Schmedemann et al. (in this issue), and in this work, size-frequency distributions (SFDs) were plotted cumulatively in the Craterstats2 program (Michael and Neukum, 2010). Absolute ages were determined for counts using the third iteration of the production and chronology functions developed by Schmedemann et al. (in this issue). The crater production function for Vesta is based on the lunar production function (derived from measuring craters over different units on the Moon, Neukum and Ivanov, 1994), which is scaled to impact conditions on Vesta. This technique uses the whole range of observed crater sizes on the well-investigated lunar surface and results in reliable slopes of the Vestan crater distribution, especially at small diameters. The lunar chronology (Neukum and Ivanov, 1994) is scaled to Vestan impact conditions, which are characterized by a factor of about 4 lower impact velocities and about 30 times higher impact flux when compared to the Moon.

In general, the current iteration of the production function fits well at diameter ranges from 50 m up to 500 km, except for in areas older than the Rheasilvia impact structure. For these, crater counts between 8 and ~ 30 –50 km are significantly below the production function. In this size range it is possible that a multitude of different effects may be observed, caused by the formation of Veneneia and Rheasilvia. These effects include multiple resurfacing events on a global scale as well as additional possibly intense but short lived cratering by the Vestan collisional family (vestoids). Schmedemann et al. (in this issue) discuss this matter in more detail. These effects are not observed on younger surfaces (< 2 Ga) like the current surface of the Rheasilvia Formation, where the observed crater size-frequency distribution closely follows the Vestan crater production function up to ~ 30 km crater size. The chronology function used in this method appears fairly accurate as it gives surface ages of the large units (Rheasilvia, Veneneia, global resurfacing) close to the peaks of the Ar–Ar age probability plot by Bogard (2011).

7.2. Method 2

An independent assessment of the cratering record of five units of Vesta has been carried out using the crater catalog of Marchi et al. (2012a). The crater retention ages of these terrains have been

derived using the Model Production Function (MPF) (Marchi et al., 2012a, 2012b, 2012c, in this issue). In this method, the current impact rate on Vesta is computed using a model main belt size-frequency distribution (Bottke et al., 2005). Then, a Pi-group crater scaling law (Holsapple and Housen, 2007) is used to convert the current impact flux in a crater production function. This gives the cumulative number of craters as a function of crater size per unit time and unit surface. Finally, the chronology function derived by O'Brien et al. (in this issue) has been used to model the impact flux at Vesta in the past. The resulting crater SFDs are shown in Fig. 23, along with some examples of MPFs.

7.3. Results and comparison

Absolute ages for units as derived by method 1 are shown in Fig. 24. We note that individual material units could be characterized by many different formation ages. Here we give average ages for the presented material units from our counts. In some cases, we also include the ages of smaller key areas inside the global units, reported by Schmedemann et al. (2012, in this issue), in order to illustrate the range of ages that have been reported within the material units.

The Rheasilvia mound (Rm) terrain yields an average age of 1.78 ± 0.32 Ga. However, the formation age of the Rheasilvia mound may also be estimated by examining a small area on top of the mound. This small area gives a significantly higher age of $3.59 (+0.079/-0.18)$ Ga. The lower average age likely results from repeated mass wasting, activity that did not affect the very top of the central mound significantly. For the Rheasilvia ridge-and-groove terrain (Rrg), we determined an age of 2.03 ± 0.18 Ga, similar to the Rheasilvia smooth terrain (Rs), with an average age of 2.03 ± 0.11 Ga. In the range of Matronalia Rupes and in the eastern part of the Veneneia impact structure the Rs unit has older surface ages, around 3.4 Ga (Veneneia floor: $3.39 + 0.098/-0.25$ Ga) (Schmedemann et al., in this issue).

The cratered plains (cp) have an average age of $2.98 + 0.18/-0.28$ Ga and the Divalia Fossae unit (Df) has an average age of 3.36 ± 0.03 Ga. For the cratered highlands (ch), we calculated an average age of 3.42 ± 0.01 Ga, and for the Saturnalia Fossae unit (Sf), we calculated an average age of $3.46 + 0.12/-0.59 \pm 0.02$ Ga. A correlation of units is shown in Fig. 25.

In this work, utilizing a methodology based on Schmedemann et al. (in this issue), we counted a similar number of craters as Marchi et al. (in this issue). Differences in ages are due mainly to the use of the different production functions, so we note caveats for both methods here. Counts by Schmedemann et al. (in this issue) include additional large craters identified solely by topographic signature, resulting in older ages for some units. The crater SFDs shown in Fig. 24 exhibit wavy shapes that differ significantly from the shape of the crater SFDs for the Rheasilvia floor. They also differ from the shape of the model production function. This could be explained by a past impact SFD significantly different from the present (a hypothesis not supported by crater SFD from other asteroids, Marchi et al., in this issue), or collisional evolution models (Bottke et al., 2005). Alternately, the geologic units may not define regions with uniform crater retention ages. Finally, the most heavily cratered terrains on Vesta may have reached a state of quasi-equilibrium (Gault, 1970), where newly formed craters have erased significantly older craters. In this case, the cratering retention ages would represent lower limits for the true age of the surface.

Though beyond the scope of this work, it is clear that age assessments of the various units and subunits (particularly ch, Df and Sf) need further investigation. In support of that work, we will continue our crater counting efforts with the goal of having a complete crater catalog down to diameters of 500 m.

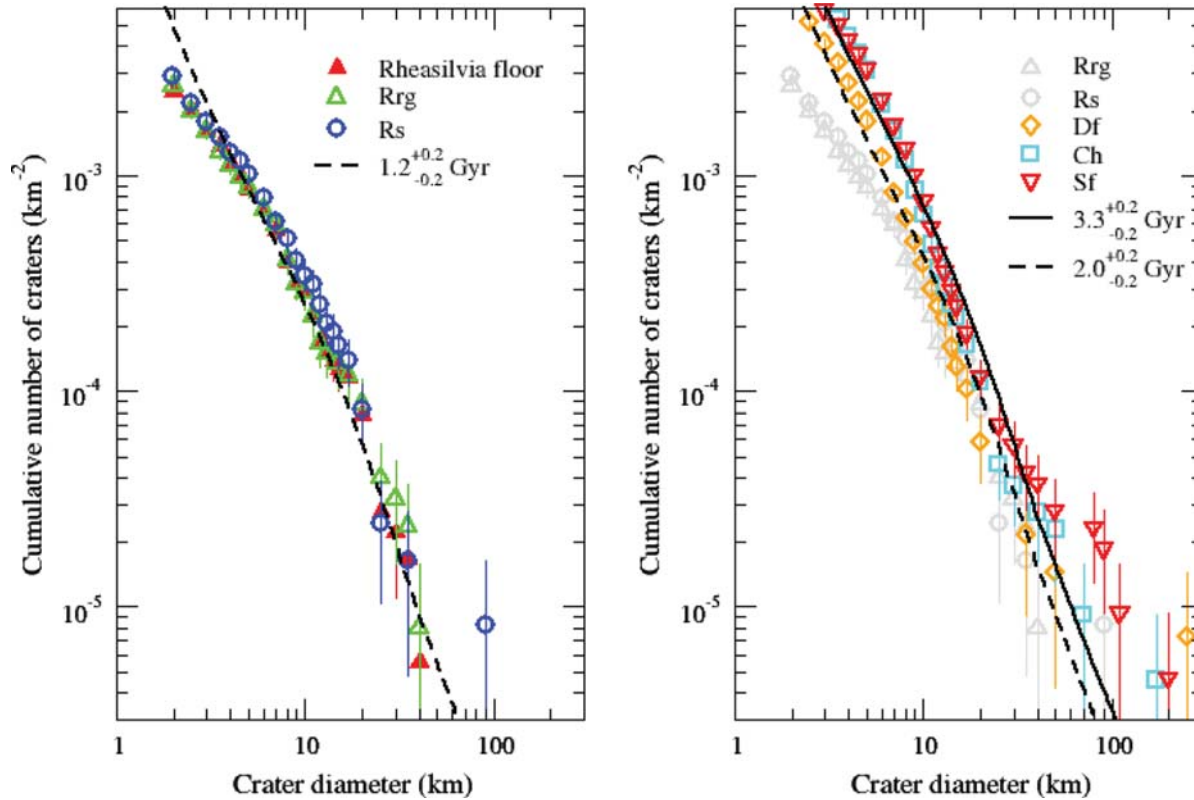


Fig. 23. Crater statistics data based on the method of Marchi et al. (2012a). The left panel shows the model production function best fit of the Rrg unit which results in an age of $\sim 1.2 \pm 0.2$ Ga. The right panel shows the crater SFDs for Sf, ch, and Df units. The age for Rrg is slightly higher than a previous estimate of $\sim 1.0 \pm 0.2$ Ga based on Rheasilvia whole floor counts (from Marchi et al., 2012a). The difference is due to a better definition of the counting area: the average crater density on Rrg unit is slightly higher than the average over the whole Rheasilvia floor. This figure shows that the MPF reproduces relatively well the shape of the crater SFD (see Marchi et al., in this issue for more details). The apparent lack of crater < 3.5 km is ascribed to incomplete crater identification.

8. Geologic history

A sequence of geologic events is listed below based on the above observations and interpretations. Ages given are those calculated in this work; we refer the reader to Marchi et al. (in this issue) and Schmedemann et al. (in this issue) for comprehensive crater statistics data and results.

1. Differentiation, fractionation and crystallization of a primary crust, ~ 4 Ga (this is a time horizon, defining the oldest craters, rather than an absolute date). Formation of the oldest impact craters; this sequence is represented by the cratered highlands and plains, and Vestalia Terra is interpreted to be a remnant of this crust. We calculated an age of ~ 3.36 – 2.40 Ga for these units, but note that there is a discrepancy between the morphology and superposition relationships that indicate the greater age of cratered highlands and plains compared to the Saturnalia Fossae unit and Veneneia impact structure (3.36 and 2.40 Ga versus 3.38 Ga respectively). We expect the crater statistics for the more northern regions to be refined as these last-acquired images are analyzed.
2. Formation of Veneneia (~ 3.78 Ga based on Schmedemann et al., in this issue) and the Saturnalia Fossae unit, followed by the Rheasilvia impact event (~ 3.55 Ga based on Schmedemann et al., in this issue) and associated Divalia Fossae unit. Both events likely resulted in global resurfacing.
3. Subsequent impacts and mass movement events that subdued impact craters, complex crater rims and portions of ridge-and-trough sets, and formed slumps and landslides, especially within crater floors and along rims and scarps. Subsequent to the Rheasilvia Formation, discontinuous low-albedo deposits

formed or were emplaced. The latest features to be formed were craters with bright rays, and surface features such as dark mantle material.

9. Lessons learned through the mapping process

The Dawn at Vesta mission has provided a unique opportunity to not only geologically map globally a small, sub-spherical, airless rocky body using high-resolution data, but to record and analyze the mapping process during that mission, to better identify best practices under such circumstances. Lessons learned during this process are reported in this section.

9.1. Iterative mapping process during data acquisition

Executed progressively throughout data acquisition, the mapping process provided the team with geologic proto-units in a timely manner. Rapid data acquisition, and the consequent need to generate new products quickly, led us to three conclusions.

Firstly, though the original plan was for two individuals to conduct the iterative mapping throughout the data acquisition phase of the mission, in execution we chose to divide the labor between four mappers. This plan worked better than two would have done, as products were demanded by the team nearly as quickly as four people could produce them. We thus recommend that similar efforts to create global geologic maps during data acquisition employ at least three or four experienced mappers. We note that for a body of this size, we found the division of labor that we adopted to be effective (one mapper for each pole, and one

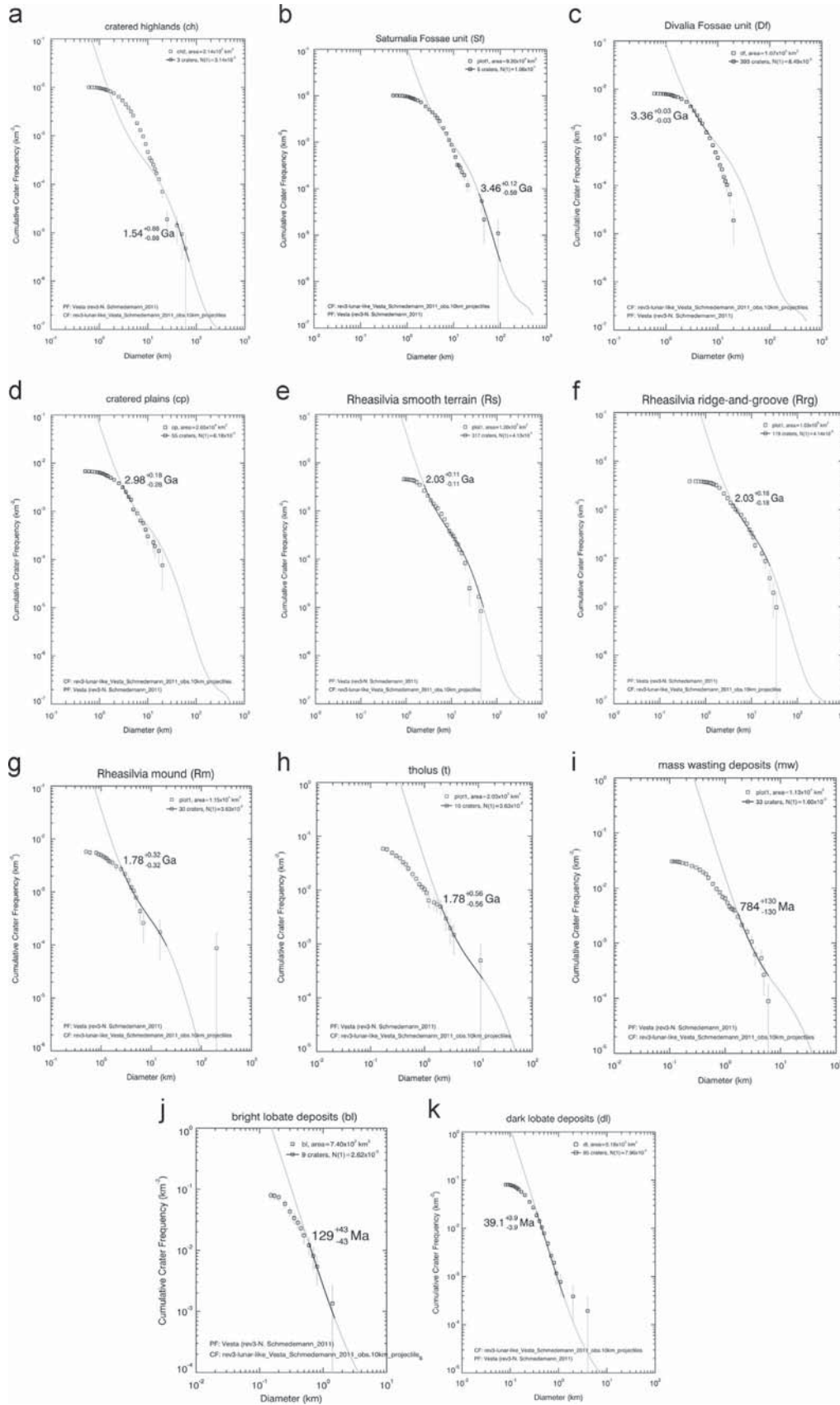


Fig. 24. Crater size-frequency distribution functions for the major geologic units described. (a) ch; (b) Sf; (c) Df; (d) cp; (e) Rs; (f) Rrg; (g) Rm; (h) mw; (i) t; (j) bl; and (k) dl.

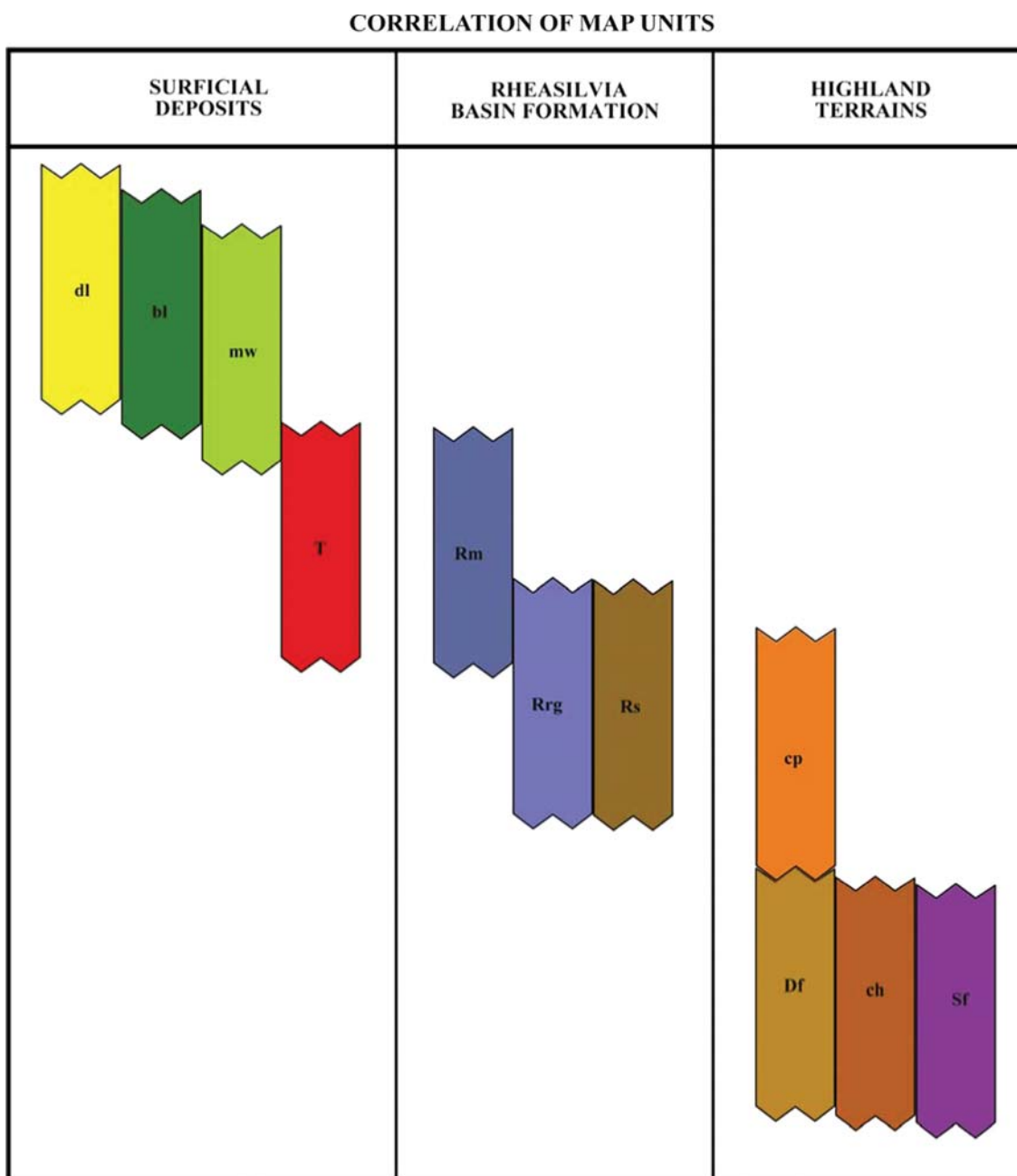


Fig. 25. Column showing the correlation of material units as a function of time. Age decreases from the bottom to the top of the figure.

each for the east and west equatorial regions, with that individual changing between each data acquisition phase).

Secondly, we found that experience, both in mapping and in identifying and interpreting the types of features that were present, was a crucial factor in producing rapidly a global geologic map that provided information about coherent units connected by similar process. We found that less experience in the process tended to lead to maps that grouped disconnected features, or to mapping features extraneous to the science questions driving map production. Additionally, the experienced mappers were able to work more quickly by using standard approaches with which they were already familiar, and were able to discuss and debate similarities and difference between mapped regions more efficiently. This efficiency was improved when discussions of early map drafts included individuals having strong expertise in modeling the types of features we were identifying. The radial scarps in the Rheasilvia impact structure were identified as early as OpNav

(Fig. 2); similarly, the shape and morphology of the “grooved” terrain was interpreted to be ridges and grooves by team members who were familiar with the processes predicted to create such features, and thus knew what clues to look for to identify and discriminate them from other linear features such as graben, scarps, or crater chains. The ability to draw from a team’s broad expertise greatly improved our ability to map accurately and efficiently.

Thirdly, we found that the minimal time between data acquisition and product generation meant that overthinking was minimized among the mappers. On the other hand, the pressure upon the global mapping team was enormous to produce precise unit boundaries that fed into other investigations (crater counting statistics, for example, or other mapping projects), as rapidly as possible. This pressure drove the mapping team to retain shortcuts longer than they might have been ideally used. For example, the team retained much of the standardized nomenclature and symbology

originally adopted as a preliminary step, rather than allowing unit definitions and nomenclature to evolve more organically with each iteration. We believe that interpretation of the resulting map was hampered by the necessity to provide the team with a standard nomenclature and symbology early in the process, and we might have learned more about the unique features of Vesta if we had been less driven by the mission timeline to formalize features and symbology quickly. We thus recommend retaining generic descriptors and symbology for as long as possible into the global mapping process.

9.2. Mapping and interpreting units

The process of mapping and interpreting units was affected by both the intermittent acquisition of new data and the nature of the data acquired. We noted three important ways in which this was the case.

Firstly, as detailed in Section 4.1, RC/OpNav allowed us to identify some of the major features on Vesta, though we identified most units and determined most general boundaries using Survey data. However, there were some changes made to the units between acquisition of Survey and HAMO data. One notable one was the nature of the boundaries of Vestalia Terra; it was not clear until HAMO data was acquired, whether or not the majority of the boundaries around this rise were scarps. Through HAMO, as well, the mappers debated whether the cratered plains were a discrete unit, and if so, what their boundaries were and how they could be defined. Of all the units listed in Fig. 5, it is the identification and boundaries of cratered plains of which we are most unsure, and a more definitive characterization of this unit may require fully calibrated and interpreted mineralogic data.

Secondly, and related to this issue, the fact that fully calibrated VIR multispectral data was not available was a hindrance to the mapping process and subsequent interpretation. On a body like Vesta, where few clues exist to distinguish one cratered terrain from another besides crater density, this was especially true. Additionally, without a way to estimate the mineralogy of crater ejecta we could not utilize craters as probes into the composition of the subsurface. Ultimately we were never able to use VIR multispectral to define or refine units, only to more specifically describe units.

Thirdly, in comparing our resulting map derived from RC/OpNav data to those derived from other iterations of the map, it was clear that when only coarse resolution was available, features with a larger topographic range, such as craters, and ridges and troughs, were easier to identify than other features and terrains. Not every interpretation based on topography was correct; we interpreted the combined rims of Marcia, Calpurnia and Minucia (seen in Fig. 3) as a single large, individual scarp (Fig. 2). However, topography and shadow played a more important role in correct identification than morphology, especially where boundaries were raised (e.g., Vestalia Terra). We believe this is in part because topographic variations are greater on Vesta than on many previously mapped terrestrial bodies; for example, Vesta's ratio of surface relief to radius is $\sim 15\%$, compared to $\sim 1\%$ for the Moon and Mars (Jaumann et al., 2012). Other units, and thus the potential processes from which they stem, were difficult to identify or interpret based solely on differences in morphology or albedo. For example, the Rheasilvia smooth member (Rs) and the Rheasilvia ridge-and groove member (Rrg) were noted in the RC/OpNav map in Fig. 2 as D2 and D1 respectively, but the boundaries were mapped as uncertain and the units themselves were difficult to interpret. In summary, we believe that for small, irregular bodies, topography is a more discriminating characteristic than morphology for identifying and characterizing features and units, especially when the available resolution is very coarse.

Acknowledgments

The authors are grateful to Corey Fortezzo, Trent Hare, Jenny Blue and other personnel at USGS for their invaluable discussions and for creating the ArcGIS base materials that greatly simplified the mapping process. Thanks go especially to the Dawn operations, engineering and science team. The authors also gratefully acknowledge the insightful comments of Drs. Jim Zimbelman and Jim Skinner, whose reviews greatly improved this manuscript. This work was funded through NASA Dawn at Vesta Participating Scientist Program Grant NNX10AR19G to RAY. Italian co-authors were funded through the Italian Space Agency (ASI) Grant 1/004/12/0.

References

- Batson, R.M., 1990. Map formats and projections used in planetary cartography. In: Greeley, R., Batson, R.M. (Eds.), *Planetary Mapping*. Cambridge Univ. Press, New York, USA, pp. 266–267.
- Binzel, R.P., Xu, S., 1993. Chips off of asteroid 4 Vesta: evidence for the parent body of achondrite meteorites. *Science* 260, 186–191.
- Binzel, R.P., Gaffey, M.J., Thomas, P.C., Zellner, B.H., Storrs, A.D., Wells, E.N., 1997. Geologic mapping of Vesta from 1994 Hubble Space Telescope images. *Icarus* 128, 95–103.
- Bogard, D.D., 2011. K–Ar ages of meteorites: clues to parent-body thermal histories. *Chem. – Geochem.* 71 (3), 207–226.
- Botke, W.F., Durda, D.D., Nesvorný, D., Jedicke, R., Morbidelli, A., Vokrouhlický, D., Levison, H., 2005. The fossilized size distribution of the main asteroid belt. *Icarus* 175, 111–140.
- Buczkowski, D.L., Wyrick, D.Y., Iyer, K.A., Kahn, E.G., Scully, J.E.C., Nathues, A., Gaskell, R.W., Roatsch, T., Preusker, F., Schenk, P.M., Le Corre, L., Reddy, V., Yingst, R.A., Mest, S., Williams, D.A., Garry, W.B., Barnouin, O.S., Jaumann, R., Raymond, C.A., Russell, C.T., 2012. Large-scale troughs on Vesta: a signature of planetary tectonics. *Geophys. Res. Lett.* 39, L18205, <http://dx.doi.org/10.1029/2012GL052959>.
- Buczkowski, D.L., Barnouin-Jha, O.S., Prockter, L.M., 2008. 433 Eros lineaments: global mapping and analysis. *Icarus* 193 (1), 39–52.
- Consolmagno, G.J., Drake, M.J., 1977. Composition and evolution of the eucrite parent body: evidence from rare earth elements. *Geochim. Cosmochim. Acta* 41, 1271–1282.
- Degewij, J., Tedesco, E.F., Zellner, B., 1979. Albedo and color contrasts on asteroid surfaces. *Icarus* 40, 364–374.
- Denevi, B.W., Blewett, D.T., Buczkowski, D.L., Capaccioni, F., Capria, M.T., De Sanctis, M.C., Garry, W.B., Gaskell, R.W., Le Corre, L., Li, J.-Y., Marchi, S., McCoy, T.J., Nathues, A., O'Brien, D.P., Petro, N.E., Pieters, C.M., Preusker, F., Raymond, C.A., Reddy, V., Russell, C.T., Schenk, P., Scully, J.E.C., Sunshine, J.M., Tosi, F., Williams, D.A., Wyrick, D., 2012. Pitted terrain on Vesta and implications for the presence of volatiles. *Science* 338, 246–249.
- De Sanctis, M.C., Coradini, A., Ammannito, E., Filacchione, G., Capria, M.T., Fonte, S., Magni, E., Barbis, A., Bini, A., Dami, M., Fici-Veltroni, I., Preti, G., the VIR team, 2011. The VIR spectrometer. *Space Sci. Rev.* 163, 329–369.
- De Sanctis, M.C., Nathues, A., Ammannito, E., Capaccioni, F., Frigeri, A., Le Corre, L., Jaumann, R., Palomba, E., Pieters, C.M., Reddy, V., Stephan, K., Tosi, F., Yingst, A., Zambon, F., Barucci, M.A., Blewett, D.T., Capria, M.T., Combe, J.-Ph., Denevi, B.W., Keller, H.U., Marchi, S., McCord, T.B., McFadden, L.A., McSween, H., Raymond, C.A., Russell, C.T., Sunshine, J., Toplis, M., Li, J.-Y., 2012. First mineralogical maps of 4 Vesta. In: 43rd Lunar and Planetary Science Conference, Abstract #1902.
- Dietz, R.S., 1946. The meteoritic impact origin of the Moon's surface features. *J. Geol.* 54, 359–375.
- Fujiwara, A., Asada, N., 1983. Impact fracture patterns on Phobos ellipsoids. *Icarus* 56, 590–602.
- Gaffey, M.J., 1983. The asteroid (4) Vesta: rotational spectral variations, surface material heterogeneity, and implications for the origins of basaltic achondrites. In: 14th Lunar and Planetary Science Conference, pp. 231–232.
- Gaffey, M.J., 1997. Surface lithologic heterogeneity of Asteroid 4 Vesta. *Icarus* 127, 130–157.
- Gault, D.E., 1970. Saturation and equilibrium conditions for impact cratering on the lunar surface: criteria and implications. *Radio Sci.* 5, 273–291.
- Greeley, R., Batson, R.M., 1990. *Planetary Mapping*. Cambridge Univ. Press p. 296.
- Hartmann, W.K., 1966a. Martian cratering. *Icarus* 5, 565–576.
- Hartmann, W.K., 1966b. Early lunar cratering. *Icarus* 5, 406–418.
- Hartmann, W.K., Neukum, G., 2001. Cratering chronology and evolution of Mars. In: Kallenbach, R., Geiss, J., Hartmann, W.K. (Eds.), *Chronology and Evolution of Mars*. Kluwer Press and International Space Science Institute, The Netherlands, pp. 165–194.
- Holsapple, K.A., Hausen, K.R., 2007. A crater and its ejecta: an interpretation of Deep Impact. *Icarus* 187, 345–356.
- Jaumann, R., Williams, D.A., Buczkowski, D.L., Yingst, R.A., Preusker, F., Hiesinger, H., Schmedemann, N., Kneissl, T., Vincent, J.B., Blewett, D.T., Buratti, B.J., Carsenty, U., Denevi, B.W., De Sanctis, M.C., Garry, W.B., Keller, H.U., Kersten, E., Krohn, K., Li, J.-Y., Marchi, S., Matz, K.D., McCord, T.B., McSween, H.Y., Mest, S.C., Mittlefehldt, D.W., Mottola, S., Nathues, A., Neukum, G., O'Brien, D.P., Pieters, C.M., Prettyman, T.H.,

- Raymond, K., Roatsch, T., Russell, C.T., Schenk, P., Schmidt, B.E., Scholten, F., Stephan, K., Sykes, M.V., Tricario, P., Wagner, R., Zuber, M.T., Sierks, H., 2012. Vesta's shape and morphology. *Science* 336, 687–690. <http://dx.doi.org/10.1126/science.1219122>.
- Jutzi, M., Asphaug, E., 2011. Mega-ejecta on asteroid Vesta. *Geophys. Res. Lett.* 38, <http://dx.doi.org/10.1029/2010GL045517>.
- Keller, H.U., et al., 2010. E-type asteroid (2867) Steins as imaged by OSIRIS on board Rosetta. *Science* 327, 190–193. <http://dx.doi.org/10.1126/science.1179559>.
- Kneissl, T., van Gassel, S., Neukum, G., 2011. Map-projection-independent crater size-frequency determination in GIS environments – new software tool for ArcGIS. *Planet. Space Sci.* 59, 1243–1254.
- Krohn, K., Jaumann, R., Stephan, K., Elbeshausen, D., Preusker, F., Roatsch, T., Otto, K., Matz, K.D., Raymond, C.A., Russell, C.T., 2012. Unusual bimodal craters on slopes, Vesta. In: 7th European Planetary Science Conference, Abstract EPSC2012-463-3.
- Li, J.-Y., McFadden, L.A., Parker, J.W.m., Young, E.F., Stern, S.A., Thomas, P.C., Russell, C.T., Sykes, M.V., 2006. Photometric analysis of 1 Ceres and surface mapping from HST observations. *Icarus* 182, 143–160.
- Li, J.-Y., McFadden, L.A., Thomas, P.C., Mutchler, M., Parker, J.W.m., Young, E.F., Russell, C.T., Sykes, M.V., Schmidt, B., 2008. Photometric mapping of asteroid (4) Vesta from HST observations. In: 39th Lunar and Planetary Science Conference, Abstract #2253.
- Li, J.-Y., McFadden, L.A., Thomas, P.C., Mutchler, M.J., Parker, J.W., Young, E.F., Russell, C.T., Sykes, M.V., Schmidt, B.E., 2010. Photometric mapping of Asteroid (4) Vesta's southern hemisphere with Hubble Space Telescope. *Icarus* 208, 238–251.
- Lugmair, G.W., Shukolyukov, A., 1998. Early solar system timescales according to ^{53}Mn – ^{53}Cr systematics. *Geochim. Cosmochim. Acta* 62, 2863–2886.
- Marchi, S., McSween, H.Y., O'Brien, D.P., Schenk, P., De Sanctis, M.C., Gaskell, R., Jaumann, R., Mottola, S., Preusker, F., Raymond, C.A., Roatsch, T., Russell, C.T., 2012a. The violent collisional history of Asteroid 4 Vesta. *Science* 336, 690–694.
- Marchi, S., Massironi, M., Vincent, J.-B., Morbidelli, A., Mottola, S., Marzari, F., Koppers, M., Besse, S., Thomas, N., Barbieri, C., Naletto, G., Sierks, H., 2012b. The cratering history of asteroid (21) Lutetia. *Planet. Space Sci.* 66, 87–95.
- Marchi, S., McSween, H.Y., O'Brien, D., Schenk, P., De Sanctis, M.C., Gaskell, R., Hiesinger, H., Jaumann, R., Mottola, S., Preusker, F., Raymond, C.A., Roatsch, T., Russell, C.T., Yingst, R.A., 2012c. Vesta collisional history revealed by Dawn: building a Vesta global crater catalog. In: 43rd Lunar and Planetary Science Conference, Abstract #1617.
- McCord, T.B., Adams, J.B., Johnson, T.V., 1970. Asteroid Vesta: Spectral reflectivity and compositional implications. *Science* 168, 1445–1447.
- McCord, T.B., Li, J.-Y., Combe, J., -Ph., McSween, H.Y., Jaumann, R., Reddy, V., Tosi, F., Williams, D.A., Blewett, D.T., Turrini, D., Palomba, E., Pieters, C.M., De Sanctis, M.C.E., Ammannito, E., Capria, M.T., Le Corre, L., Longobardo, A., Nathues, A., Mittlefehldt, D.W., Schröder, S.E., Hiesinger, H., Beck, A.W., Capaccioni, F., Carsenty, U., Keller, U., Denevi, B.W., Sunshine, J.M., Raymond, C.A., Russell, C.T., 2012. Dark Material on Vesta from the infall of carbonaceous volatile-rich material. *Nature* 491, 83–86. <http://dx.doi.org/10.1038/nature11561>.
- McSween Jr., H.Y., Mittlefehldt, D.W., Beck, A.W., Mayne, R.G., McCoy, T.J., 2011. HED meteorites and their relationship to the geology of Vesta and the Dawn Mission. *Space Sci. Rev.* 163, 141–174. <http://dx.doi.org/10.1007/s11214-010-9637-z>.
- Michael, G.G., Neukum, G., 2010. Planetary surface dating from crater size-frequency distribution measurements: partial resurfacing events and statistical age uncertainty. *Earth Planet. Sci. Lett.* 294, 223–229.
- Neukum, G., Ivanov, B.A., 1994. Crater size distributions and impact probabilities on Earth from lunar, terrestrial-planet, and asteroid cratering data. In: Gehrels, T., Matthews, M.S., Schumann, A. (Eds.), *Hazards due to Comets and Asteroids*, Space Science Series. University of Arizona Press, Tucson, AZ, p. 359.
- Nyquist, L.E., Bogard, D., Takeda, H., Bansal, B., Wiesmann, H., Shih, C.-Y., 1997. Crystallization, recrystallization, and impact-metamorphic ages of eucrites Y792510 and Y791186. *Geochim. Cosmochim. Acta* 61, 2119–2138.
- Pieters, C.M., Ammannito, E., Blewett, D.T., Denevi, B.W., De Sanctis, M.C., Gaffey, M.J., Le Corre, L., Li, J.-Y., Marchi, S., McCord, T.B., McFadden, L.A., Mittlefehldt, D.W., Nathues, A., Palmer, E., Reddy, V., Raymond, C.A., Russell, C.T., 2012. Distinctive space weathering on Vesta captures regolith mixing processes. *Nature* <http://dx.doi.org/10.1038/nature11534>.
- Polansky, C.A., Joy, S.P., Raymond, C.A., 2011. Dawn science planning, operations and archiving. *Space Sci. Rev.* 163, 511–543.
- Prettyman, T.H., Mittlefehldt, D.W., Yamashita, N., Lawrence, D.J., Beck, A.W., Feldman, W.C., McCoy, T.J., McSween, H.Y., Toplis, M.J., Titus, T.N., Tricarico, P., Reedy, R.C., Hendricks, J.S., Forni, O., Le Corre, L., Li, J.-Y., Mizzon, H., Reddy, V., Raymond, C.A., Russell, C.T., 2012. Elemental mapping by Dawn reveals exogenic H in Vesta's regolith. *Science* 338, 242–246.
- Preusker, F., Scholten, F., Matz, K.-D., Jaumann, R., Roatsch, T., Raymond, C.A., Russell, C.T., 2012. Topography of Vesta from Dawn FC stereo images. In: 43rd Lunar and Planetary Science Conference, Abstract #2012.
- Prockter, L., Thomas, P., Robinson, M., Joseph, J., Milne, A., Bussey, B., Veverka, J., Cheng, A., 2002. Surface expressions of structural features on Eros. *Icarus* 155, 75–93.
- Raymond, C.A., Park, R.S., Asmar, S.W., Konopliv, A.S., Buczkowski, D.L., De Sanctis, M.C., McSween, H.Y., Russell, C.T., Jaumann, R., Preusker, F., 2013. Vestalia Terra: an ancient mascon in the southern hemisphere of Vesta. In: 44th Lunar and Planetary Science Conference, Abstract #2882.
- Reddy, V., Gaffey, M.J., Kelley, M.S., Nathues, A., Li, J.-Y., Yarbrough, R., 2010. Compositional heterogeneity of Asteroid 4 Vesta's southern hemisphere: implications for the Dawn Mission. *Icarus* 210, 693–706.
- Reddy, V., Nathues, A., Le Corre, L., Sierks, H., Li, J.-Y., Gaskell, R., McCoy, T., Beck, A.W., Schroeder, S.E., Pieters, C.M., Becker, K.J., Buratti, B.J., Denevi, B., Blewett, D.T., Christensen, U., Gaffey, M.J., Gutierrez-Marques, P., Hicks, M., Keller, U., Maue, T., Mottola, S., McFadden, L.A., McSween, H.Y., Mittlefehldt, D., O'Brien, D.P., Raymond, C., Russell, C., 2012a. Color and albedo heterogeneity of Vesta from Dawn. *Science* 336, 700–704.
- Reddy, V., Le Corre, L., O'Brien, D.P., Nathues, A., Cloutis, E.A., Durda, D.D., Bottke, W.F., Bhatt, M.U., Nesvorný, D., Buczkowski, D., Scully, J.E.C., Palmer, E.M., Sierks, H., Mann, P.J., Becker, K.J., Beck, A.W., Mittlefehldt, D., Li, J.-Y., Gaskell, R., Russell, C.T., Gaffey, M.J., McSween, H.Y., McCord, T.B., Combe, J.-P., Blewett, D., 2012b. Delivery of dark material to Vesta via carbonaceous chondritic impacts. *Icarus* 221, 544–559.
- Reddy, V., Li, J.-Y., Le Corre, L., Scully, J.E.C., Gaskell, R., Russell, C.T., Park, R.S., McFadden, L.A., Raymond, C., Nathues, A., Gaffey, M.J., Becker, K.J., Thangjam, G.S., 2013. Comparing Dawn, Hubble Space Telescope, ground-based interpretations of Vesta. *Icarus* 226 (1), 1103–1114.
- Reimold, W.U., Brandt, D., Koerber, C., 1998. Detailed structural analysis of the rim of a large complex impact crater: Bosumtwi Crater, Ghana. *Geology* 26, 543–546.
- Roatsch, T., Kersten, E., Matz, K.-D., Preusker, F., Scholten, F., Jaumann, R., Raymond, C.A., Russell, C.T., 2012. High resolution Vesta High Altitude Mapping Orbit (HAMO) Atlas derived from Dawn framing camera images. *Planet. Space Sci.* 73, 283–286.
- Russell, C.T., Raymond, C.A., Fraschetti, T.C., Raymond, M.D., Polansky, C.A., Schimmels, K.A., Joy, S.P., 2005. Dawn mission and operations. In: Proceedings of IAU Symposium 229, doi:10.1017/S1743921305006691.
- Russell, C.T., Raymond, C.A., Coradini, A., McSween, H.Y., Zuber, M.T., Nathues, A., De Sanctis, M.C., Jaumann, R., Konopliv, A.S., Preusker, F., Asmar, S.W., Park, R.S., Gaskell, R., Keller, H.U., Mottola, S., Roatsch, T., Scully, J.E.C., Smith, D.E., Tricarico, P., Toplis, M.J., Christensen, U.R., Feldman, W.C., Lawrence, D.J., McCoy, T.J., Prettyman, T.H., Reedy, R.C., Sykes, M.V., Titus, T.N., 2012. Dawn at Vesta: testing the protoplanetary paradigm. *Science*, 684–686. <http://dx.doi.org/10.1126/science.1219122>.
- Sasaki, S., 27 others, 2006. Observations of 25143 Itokawa by the Asteroid Multi-band Imaging Camera (AMICA) of Hayabusa: morphology of brighter and darker areas. In: 37th Lunar and Planetary Science Conference, Abstract 1671.
- Schenk, P., O'Brien, D.P., Marchi, S., Gaskell, R., Preusker, F., Roatsch, T., Jaumann, R., Buczkowski, D., McCord, T., McSween, H.Y., Williams, D.A., Yingst, R.A., Raymond, C., Russell, C.T., 2012. The giant Rheasilvia impact basin, the evolution of asteroid 4 Vesta and its link to meteorites. *Science* 336, 694–697.
- Schiller, M., Baker, J.A., Bizzarro, M., 2010. 26Al–26Mg dating of asteroidal magmatism in the young solar system. *Geochim. Cosmochim. Acta* 74, 4844–4864.
- Schmedemann, N., Kneissl, T., Ivanov, B., Michael, G., Wagner, R., Neukum, G., Ruesch, O., Hiesinger, H., Krohn, K., Roatsch, T., Sierks, H., Jaumann, R., Reddy, V., Nathues, A., Raymond, C.A., Russell, C.T., 2012. Crater size-frequency distribution (CSFD) and chronology of Vesta – crater counts matching HED Ages. In: 43rd Lunar and Planetary Science Conference, Abstract #2544.
- Shoemaker, E.M., Hackman, R.J., 1962. Stratigraphic basis for a lunar time scale. In: Kopal, Z., Mikhailov, Z.K. (Eds.), *The Moon*, Internat. Astronomical Union Symposium 14, Academic Press, London, UK, pp. 289–300.
- Sierks, H., Keller, H.U., Jaumann, R., Michalik, H., Behnke, T., Bubenhausen, F., Buttner, I., Carsenty, U., Christensen, U., Enge, R., Fiethe, B., Gutierrez Marques, P., Hartwig, H., Kruger, H., Kuhne, W., Maue, T., Mottola, S., Nathues, A., Reiche, K.-U., Richards, M. L., Roatsch, T., Schroder, S.E., Szemerey, I., Tschentscher, M., 2011. The Dawn Framing Camera. *Space Sci. Rev.* 163, 263–327.
- Sullivan, R., Greeley, R., Pappalardo, R., Asphaug, E., Moore, J.M., Morrison, D., Belton, M.J.S., Carr, M., Chapman, C.R., Geissler, P., Greenberg, R., Granahan, J., Head, J.W., Kirk, R., McEwen, A., Lee, P., Thomas, P.C., Veverka, J., 1996. *Geology of 243 Ida*. *Icarus* 120, 119–139.
- Tanaka, K.L., Moore, H.H., Schaber, G.G., Chapman, M.C., Stofan, E.R., Campbell, D.B., Davis, P.A., Guest, J.E., McGill, G.E., Rogers, P.G., Saunders, R.S., Zimbelman, J.R., 1994. *The Venus Geologic Mappers Handbook*. USGS Open File Report 94-438, 66 pp.
- Tanaka, K.L., Skinner, J.A., Jr., Hare, T.M., 2010. *The Planetary Geologic Mapping Handbook*. USGS Open File Report, 21 pp.
- Tera, F., Carlson, R.W., Boctor, N.Z., 1997. Radiometric ages of basaltic achondrites and their relation to the early history of the solar system. *Geochim. Cosmochim. Acta* 61, 1713–1731.
- Thomas, P., Veverka, J., 1979. Grooves on asteroids: a prediction. *Icarus* 40, 394–405.
- Thomas, N., et al., 2012. The geomorphology of (21) Lutetia: results from the OSIRIS imaging system onboard ESA's Rosetta spacecraft. *Planet. Space Sci.* 66, 96–124.
- Thomas, P.C., Binzel, R.P., Gaffey, M.J., Storrs, A.D., Wells, E.N., Zellner, B.H., 1997a. Impact excavation on asteroid 4 Vesta: Hubble Space Telescope results. *Science* 277, 1492–1495.
- Thomas, P.C., Binzel, R.P., Gaffey, M.J., Storrs, A.W., Wells, E., Zellner, B., 1997b. Vesta: spin pole, size and shape from HST images. *Icarus* 128, 88–94.
- Wilhelms, D.E., 1972. *Geologic mapping of the second planet*. U.S. Geol. Surv. Interagency Report, Astrogeology 55.
- Wilhelms, D.E., 1990. *Geologic mapping*. In: Greeley, R., Batson, R.M. (Eds.), *Planetary Mapping*. Cambridge Univ. Press, New York, pp. 208–260.
- Wilson, L., Keil, K., 1996. Volcanic eruptions and intrusions on asteroid 4 Vesta. *J. Geophys. Res.* 101, 18,927–18,940.
- Wilson, L., Keil, K., 1997. The fate of pyroclasts produced in explosive eruptions on the asteroid 4 Vesta. *Meteoritics Planet. Sci.* 32, 813–823.

- Yingst, R.A., Williams, D.A., Garry, W.B., Mest, S.C., Petro, N.E., Buczkowski, D., Schenk, P., Jaumann, R., Pieters, C.M., Roatsch, T., Preusker, F., Nathues, A., Le Corre, L., Reddy, V., Russell, C.T., Raymond, C.A., De Sanctis, M.C., Ammannito, E., Filacchione, G., 2011. A preliminary global geologic map of Vesta based on Dawn Survey orbit data. In: Proceedings of the American Geophysical Union. Abstract P43B-0248.
- Yingst, R.A., Mest, S., Garry, W.B., Williams, D.A., Berman, D.C., Jaumann, R., Pieters, C.M., Ammannito, E., Buczkowski, D.L., De Sanctis, M.C., Frigeri, A., Le Corre, L., Preusker, F., Raymond, C.A., Reddy, V., Russell, C.T., Roatsch, T., Schenk, P.M., Dawn Team, 2012. A preliminary global geologic map of Vesta based on high-altitude mapping orbit data. In: 43rd Lunar and Planetary Science Conference, Abstract #1359.
- Zellner, B., Storrs, A.W., Wells, E., Binzel, R.P., Thomas, P.C., Gaffey, M.J., 1997. Hubble Space Telescope images of Asteroid 4 Vesta. *Icarus* 128, 83–87.